

UNIVERSIDAD COMPLUTENSE DE MADRID

FACULTAD DE CIENCIAS MATEMÁTICAS
DEPARTAMENTO DE MATEMÁTICA APLICADA



TESIS DOCTORAL

**Modelos matemáticos de reparación ósea
Mathematical models of bone repair**

MEMORIA PARA OPTAR AL GRADO DE DOCTOR

PRESENTADA POR

Luis Echeverri Delgado

Directores

Miguel Ángel Herrero
Gerardo Oleaga

Madrid, 2014

MODELOS MATEMÁTICOS DE REPARACIÓN ÓSEA MATHEMATICAL MODELS OF BONE REPAIR

MEMORIA PRESENTADA PARA OPTAR AL TÍTULO DE DOCTOR EN CIENCIAS
MATEMÁTICAS

POR:

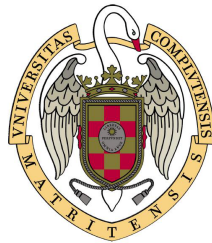
LUIS ECHEVERRI

DIRIGIDA POR:

DR. MIGUEL ÁNGEL HERRERO

Y

DR. GERARDO OLEAGA



FACULTAD DE CIENCIAS MATEMÁTICAS
DEPARTAMENTO DE MATEMÁTICA APLICADA
UNIVERSIDAD COMPLUTENSE DE MADRID

2014

Luis:-*¿y tu sabes a quien quiero yo más?*-

Ana (3 años de edad):-*“a Yo, a Yeye, y a la Abuela.”*-

Contents

Resumen	1
Abstract	5
1 Preliminaries	9
1.1 Introduction	9
1.2 Bone structure	11
1.3 Bone remodelling and the Basic Multicellular Units	13
1.4 Fracture Healing	16
1.5 Mathematical models	19
1.5.1 Mechano-regulatory models	19
1.5.2 Bio-regulatory models	20
Bibliography	23
2 Bone remodelling	29
2.1 Introduction	29
2.2 A minimal software for BMU operation	32
2.2.1 The role of molecular signals in bone remodeling	32
2.2.2 Signal integration by individual cells. Inhibitory proteins	34
2.3 Mathematical modelling	35
2.3.1 Cell algorithms	36
2.3.2 Spatial dependence in the model	41
2.3.3 Cell movements	41
2.4 Results	43
2.4.1 The BMU software proposed successfully recapitulates bone remodeling	43
2.4.2 The size of the BRC adapts to the number of apoptotic OCY	43
2.4.3 Osteoclast lifespan depends on the depth of the BRC	44
2.4.4 The BMU software is robust to signal noise	44

2.5 Discussion	46
Bibliography	49
3 Early stages of Bone fracture healing	53
3.1 Introduction	53
3.2 Basic facts on bone fracture healing. The first 48 hours	54
3.3 A mathematical model for the formation of a fibrin-collagen callus template.	57
3.3.1 Generation of fibrin monomers upon thrombin-induced fibrinogen cleavage.	58
3.3.2 Estimating fibrin clot formation	61
3.3.3 Platelet activation and growth factor release	64
3.3.4 Recruitment of mesenchymal cells (MSC). Formation of early fibrin-collagen callus (EFC)	65
3.4 A sequence of times	70
3.5 Concluding remarks	72
Bibliography	75
A Details of computer simulations of the model of BMU operation during bone remodeling	81
A.1 Time evolution of the BMU	81
A.1.1 Pseudo-code guidelines	85
B Experimental procedure	89

Resumen

En esta memoria se obtienen y analizan algunos modelos matemáticos de remodelación y reparación ósea. Para ello, y tras un primer capítulo introductorio en el que se presentan resultados preliminares para los estudios posteriores, se aborda en el Capítulo 2 la modelización del mecanismo de mantenimiento que tiene lugar a lo largo de la vida de cada persona, y en virtud del cual en pequeñas regiones del esqueleto el hueso viejo es reemplazado por el nuevo de manera que la cantidad total de hueso permanece constante.

En concreto, en el capítulo 2 se formula un modelo mínimo para el funcionamiento de las llamadas BMU (Basic Multicellular Units), grupos de células diferenciadas que actúan coordinadamente para eliminar hueso en regiones marcadas para ello (generalmente mediante señales emitidas por osteocitos, que actúan como sensores mecánicos) y a continuación generan una matriz extracelular que, tras su mineralización, da lugar al nuevo hueso que reemplaza al antiguo. La actuación de tales unidades orgánicas es conocida desde los años 60 del siglo pasado, y aunque su esquema general de actuación es conocido, y muchas de las señales químicas involucradas han sido identificadas, el mecanismo preciso por el que tales unidades se forman cuando es necesario y se deshacen una vez cumplida su tarea, sigue sin ser bien conocido.

En esta memoria proponemos un modelo operativo simple para BMUs, que se basa en las siguientes hipótesis. En primer lugar, cada célula en una BMU puede elegir una entre un número muy limitado de posibles acciones a realizar (dividirse, diferenciarse a otro tipo celular o morir). Tales decisiones no son aleatorias, sino que están reguladas por inhibidores internos específicos que bloquean cada una de esas acciones, de modo que el primero de ellos cuya concentración baja de un cierto valor crítico determina de forma irreversible la acción a seguir. La dinámica interna de estos inhibidores está modulada por señales externas, provenientes en general de otros tipos celulares presentes en la BMU. Mostramos en este capítulo que basta con un número muy pequeño de tales señales (tres) para que el proceso resulte operativo. En cualquier caso, cada célula decide individualmente lo que hace en cada momento, sin que haya ninguna determinación previa para ello, ni genética ni de otro tipo.

Sin embargo, el resultado de esta suma de decisiones individuales independientes es una acción coordinada y perfectamente regulada, que permite remodelar la zona elegida para ello de manera robusta y eficaz, como se observa mediante el análisis de los resultados obtenidos al simular el modelo correspondiente, y que se presentan en el mismo capítulo. Los resultados obtenidos permiten formular cuestiones relacionadas con la presencia detectada de un número de señales mucho mayor que las estrictamente necesarias, lo que probablemente está relacionado con conceptos como la multifuncionalidad (una misma señal induce diversos efectos en tipos celulares distintos) y la redundancia (en el sistema considerado persisten diversos mecanismos para alcanzar un resultado, que garantizan el funcionamiento del sistema cuando uno falla, pero que representan un coste metabólico para las células involucradas).

El esquema que acabamos de resumir ilustra un aspecto de la metodología seguida en esta memoria, que también se usa en el siguiente capítulo, y que nos parece particularmente relevante. En concreto, nuestro objetivo en cada uno de los problemas estudiados es obtener modelos tan simples como sea posible, que permitan reproducir los hechos observados y más aún, que proporcionen indicios sobre el funcionamiento interno de las estructuras consideradas que no han sido previamente incluidos en la formulación del modelo. Este enfoque es distinto de la estrategia habitual de modelización, que busca incluir tantos datos biológicos como sea posible en cada modelo, lo que conduce a una gran complejidad en los sistemas de ecuaciones obtenidos y en particular hace precisa la introducción de gran número de parámetros, sobre los que se sabe muy poco. Ello obliga a elegir tales parámetros para ajustar cada experimento concreto que se analiza, sin que se obtenga así un conocimiento real de la dinámica involucrada, ni se pueda explicar de manera convincente las razones de los comportamientos observados.

En el tercer capítulo de esta memoria se estudia la sucesión de procesos que tienen lugar en las etapas tempranas de la reparación del hueso después de producirse una fractura, y que son cruciales para una completa curación del mismo. Se proponen modelos matemáticos que permiten estimar los tiempos característicos de tales procesos en términos de sus parámetros cinéticos. Para ello, se analizan tales etapas de manera separada, hasta la formación del primer callo fibroso, que proporciona el molde básico sobre el que posteriores procesos de remodelación (no estudiados en esta memoria) darán finalmente lugar a nuevo tejido óseo, plenamente funcional.

El modelo propuesto es de tipo modular, de modo que consiste en una concatenación de modelos simples que se suceden uno a uno hasta completar la etapa temprana de reparación estudiada. Se comienza por describir la formación de un coágulo sanguíneo inducido por la fractura, cuya aparición se caracteriza como una transición de fase tipo sol-gel, en la que el coágulo resultante es descrito como un gel. La formación de dicho coágulo, que debe conectar los bordes de la fractura proporcionando una primera unión entre ambos, es condición necesaria para el éxito del proceso completo de reparación. Describimos en primer lugar la generación de monómeros de fibrina a partir de la activación de su precursor inactivo presente en la sangre (fibrinógeno) mediante la acción de trombina, liberada tras las roturas vasculares inducidas por una fractura. Los monómeros así formados se polimerizan

rápidamente para formar grandes agregados. Usando la teoría de polimerización clásica, el proceso correspondiente puede ser modelado por un sistema infinito de ecuaciones de coagulación-fragmentación para los k -meros con $k \geq 1$, en las que los coeficientes de coagulación son proporcionales al número de enlaces funcionales libres en cada monómero. Dado que no es posible en general resolver las ecuaciones anteriores, se recurre a la introducción de una relación de clausura para caracterizar la transición de fase buscada. Ello se hace sobre las ecuaciones para los momentos de la distribución de polímeros, en las que ahora es posible estimar de manera simple el cociente M_2/M_1 , que corresponde al tamaño medio molecular, de modo que la transición de fase buscada aparece cuando este cociente desarrolla una singularidad. Se obtienen fórmulas para el tiempo de coagulación que son explícitas en varios casos y que permiten estimar el tiempo de coagulación en el caso más general.

Por otra parte, además de romper las moléculas de fibrinógeno, la trombina activa a las plaquetas de la sangre, que cambian su forma liberando factores de crecimiento. En este capítulo se analiza el efecto inducido por un factor de crecimiento genérico g , que se difunde a través del coágulo para atraer a las células mesenquimales. Éstas juegan un importante papel en la formación del primer callo elástico, analizado en este trabajo, y que proporciona el primer molde con estructura elástica suficiente para servir de base a posteriores procesos de osificación no considerados en esta memoria.

Tras proponer un modelo de tipo clásico para la difusión de g , se obtiene una solución explícita para dicha función, cuyo gradiente provoca el movimiento por quimiotaxis de las células mesenquimales m desde el borde de la fractura hacia su interior. Se muestra que el perfil del gradiente de g se estabiliza rápidamente y puede aproximarse por una función lineal, siempre que el intervalo temporal no supere al tiempo de vida media de las plaquetas. Se obtiene así una estimación para el tiempo T_F de formación del callo fibroso, que completa las obtenidas previamente para otros tiempos característicos del proceso. Los resultados así obtenidos son finalmente comparados con los existentes en la literatura.

Abstract

This work is concerned with the mathematical modelling and simulation of bone remodelling and repair. To this end, after a first introductory chapter where a number of preliminaries are gathered, we consider in Chapter 2 the modelling of a homeostatic maintenance mechanism that is at work during a whole life, and by means of which in small, targeted regions in the skeleton old bone is first destroyed and then replaced by new one, so that the total amount of bone remains constant.

More precisely, in Chapter 2 a model for the operation of the so-called Basic Multicellular Units (BMU) is formulated. BMUs are groups of differentiated cells that act co-ordinately to destroy (resorb) bone in targeted zones, identified as such by osteocytes, that are able to act as mechanical sensors, and then secrete extracellular matrix which upon subsequent mineralization yields new bone to substitute the previous one. The existence of such organic units is known since the sixties of the former century and, while its general way of action is known, and many of the chemical messengers involved have been identified, the precise manner by which such units are formed when needed, and disbanded afterwards, remains to be ascertained as yet .

In this memoir, a simple operative model for BMU operation is proposed. It is based in the following assumptions. To begin with each cell in a BMU can only select one among a very limited choice of actions (to divide, to die or to differentiate into another cell type). Such decisions are not randomly made, but are instead regulated by specific internal inhibitors, which block each of these actions, so that the first of them that goes below a critical threshold irreversibly determines cell fate. The internal dynamics of such inhibitors is modulated by external signals, released by other cell types present in a BMU. We show that a very reduced number of such signals (actually three) suffices to keep BMU at work. In any case, each cell individually decides its course of action without resorting to any previously determined plan, genetic or otherwise. Nevertheless, the outcome of this sum of independent individual decisions turns out to be a coordinated and perfectly regulated course of action, that leads to a robust and efficient remodelling of the zone involved, as can be seen from analysis of the results obtained upon simulation of the model, that bare described

in the same chapter. The results thus obtained lead to interesting questions related to the detected presence of a set of signals much larger than that actually needed for the model. This is probably related with aspects as multi-functionality (a same signal may induce different actions in different cells) and redundancy (coexistence in a same system of different mechanisms that yield the same result, thus ensuring a security mechanisms against failure, though at the expense of a metabolic costs for the cells involved).

The pattern described above shows one of the methodology characteristics followed in this thesis, which is also used in the next chapter, and that we consider especially relevant. Namely, our goal for each of the problems under study is to obtain simple models which can recreate the observed facts. Furthermore, these simple models will provide indications on the internal behaviour of the considered structures, which had not been included previously in the formulation of the model. This approach is slightly different to the usual modelling strategy that is to include as much detail as possible, leading to typically very complex systems of equations with a large number of parameters, most of which are unknown. This forces one to identify such parameters for each specific analyzed experiment, without gaining any real knowledge on the dynamics of the problem or explanation of the observed behaviour.

In the third chapter of this thesis the processes which take place in the early stages of a fractured bone repair are studied. These early stages are crucial for the complete recovery of the bone. Mathematical models are provided to estimate the time scales of these processes as a function of their kinetic parameters. To do so the different stages are analysed separately, up to the formation of the first fibrous callus, which is the basic mould on which further remodellation processes will take place (not studied in this work). This process ends with fully functional new bone tissue.

The proposed model has a modular structure, formed by a sequence of simple models which follow one another until completing the early stages of the bone repair under study. Initially, the onset of a blood clot induced by the fracture is described as a phase transition of sol-gel type, where the clot is represented as a gel. The formation of this blood clot, which connects the edges of the fracture, is a necessary condition to ensure the repair process is successful. The first stage is the generation of fibrin monomers from the activation of their inactive precursor present in blood (fibrinogen) by the action of thrombin, which is released after the vascular breaks induced by a fracture. The monomers which have just been created polymerise rapidly to form large agglomerates. Following classical polymerisation theory, the above process can be modelled using an infinite system of coagulation-fragmentation equations for the k -mers with $k \geq 1$. The coagulation coefficients are proportional to the number of free functional bonds of each monomer. In general the mentioned equations cannot be solved, thus the introduction of a closure relation to characterise the phase transition is needed. This is done for the equations describing the moments of the distribution of polymers, for which the coefficient M_2/M_1 can be easily estimated. This coefficient describes the molecular mean size, therefore the phase transition will be present when

a singularity appears in the coefficient. Explicit formulas for the coagulation time are obtained for several cases, and these provide an estimate for coagulation time for a more general case.

Thrombin, apart from breaking fibrinogen molecules, also activates blood platelets, which change shape whilst releasing growth factors. In this chapter the effect induced by a generic g growth factor is analysed, which spreads around the clot to attract mesenchymal cells. These play an important role in the formation of the first elastic callus (analysed in this work) that provides the first elastically structured mould. This mould is the building foundation for posterior ossification processes which are not considered in this work.

A classical diffusion model for g is solved, obtaining an explicit solution. The gradient of g induces a chemotaxis movement of the mesenchymal cells m from the edge of the fracture towards the interior. The profile of the gradient of g is shown to stabilise rapidly and can be approximated by a linear function, as long as the time interval does not overcome the half-life of the platelets. In this way an estimate of T_F is obtained, which is the time of formation of the fibrous callus. This completes the estimates obtained previously for other characteristic time scales. The obtained results are compared to those found in the literature.

Preliminaries

1.1 Introduction

The human skeleton is a complex structure which provides a supporting framework for the whole body. In addition, it acts as a shield to protect internal organs, serves as a reservoir for a number of ions (particularly for calcium) and plays a crucial role in body motion by mediating the transmission of force arising from muscle contraction. Bone function is thus essential for human life, which makes important to keep bone homeostasis by preventing, and when needed repairing , all kinds of bone disorders.

Out of the many bone-related hazards, bone fracture is a particularly relevant one. About 1.5 million people suffer a bone disease-related fracture each year in the U.S [54], and recent studies claim that about 280 fragility-related fractures per hour occurred in Europe's five largest countries and Sweden in 2010 [52]. Such figures are expected to keep increasing in the future, particularly in aging societies as developed countries are.

In spite of such sobering data, it turns out that human bone has an impressive capability for self-repair. In fact, our skeleton is continuously being renewed, so that old bone is being destroyed in some places, to be eventually replaced by new bone produced in the same locations. In that manner the whole skeleton is changed every 10 to 15 years [37]. This self-renewal process, termed as bone remodeling, is known to be triggered by local changes in mechanical load, and takes place at a microscopic scale. Such repairing task is carried out in each case by a comparatively small number of cells, that make up a Basic Multicellular Unit (BMU) [18] which is mobilized for that purpose and then disbanded once its task is concluded. In fact, BMUs are recruited when osteocytes, a characteristic bone cell type, detect that mechanical stress goes locally outside of a range of admissible values [43].

A particular case in which the previous situation applies corresponds to the onset of micro-fractures . These can be induced just by physical exercise (including walking) and their occurrence (and efficient repair) is believed to significantly contribute

to keep bone remodeling in good shape [49]. However, when many micro-fracture coalesce, or when a comparatively large fracture appears (for instance, as a consequence of a traumatic event), BMUs turn out to be too small to take care of the repairing process then needed, which has to be carried out at larger space and time scales. To address the resulting new challenges, a number of strategies have been set in place in the course of evolution. In particular, inflammatory signals play now a key role and a blood clot is formed that, upon serving as a first bridge to connect fracture borders, is subsequently remodeled to produce several callus with increased stiffness, which will be eventually replaced by new bone when the process successfully concludes. It is worth to be noticed that, unlike other tissue healing processes that leave scars when concluded, bone remodeling and bone fracture repair are scar-less, so that no interface between old and new bone can be easily tracked. This seems to be related to the fact that bone healing shares several characteristics in common with the developmental program according to which ossification is carried out at the embryonic stage [20].

In this memoir we shall address two problems, each related with one of the two repairing events described before. To begin with, in our next Chapter 2 we will provide a simple mathematical model that accounts for successful BMU operation during standard, homeostatic bone remodeling. In that Chapter, BMU operation will be described as an emergent behavior that can be derived from a reduced set of assumptions on the possible individual choices of the cells involved in one hand, and on the number of effective chemical cues mediating such decisions on the other. Then in Chapter 3 we shall be concerned with fracture repair, in particular in the case of fractures small enough so that theoretical results could be compared with experimental ones, but beyond the range of BMU operation alone. In particular, the onset of a blood clot will now be crucial and has to be taken into account in the corresponding model. It will be shown there that preliminary (albeit in our opinion, illuminating) estimates on the characteristic times of the repairing mechanisms can be deduced from a simple set of assumptions concerning kinetic aspects of the early stages of the corresponding bone healing process.

We have used several times the term simplicity when describing the goals addressed in this work. Indeed, a basic pattern in our approach consists in showing that key aspects of the processes considered can be retrieved from the dynamics of mathematical models where the underlying molecular and cell mechanisms have been reduced to their minimal possible ingredients. No attempt to build comprehensive, exceedingly complex models requiring of extensive parameter fitting is made here. We have rather chosen a different path, and in each case have tried to ascertain the minimal number of mechanisms required to account for the processes considered.

The results previously sketched (in a very succinct manner) are to be found in Chapters 2 and 3, as already mentioned. The rest of this introduction is devoted to provide a number of preliminaries which will be later referred to in such Chapters. In particular, we will shortly recall a few facts about bone structure in Section 1.2 below. Additional information about bone remodeling and the role therein played by BMUs can be found in Section 1.3, whereas a brief review of facts concerning

bone fracture will be gathered in section 1.4. The emphasis in these sections is on the biological facts underlying such processes. A short discussion on the use of mathematical models to better understand the mechanisms involved is then provided in Section 1.5.

1.2 Bone structure

The skeleton in vertebrates is formed by two tissues: bone and cartilage. In humans the skeleton contains over 200 different elements that have been traditionally classified according to shape into long, short, flat and irregular bones. Cartilage is the connective tissue that can be found in the joints between bones. It is formed by cells called chondrocytes that produce a large amount of extracellular matrix of collagen fibers. One of the main differences between bone and cartilage is that bone is a highly vascularized tissue and cartilage has virtually no blood vessels [51]. In this work we are going to focus on bones and we will not study cartilage in deep.

The individual bones could be described at the macroscopic and/or microscopic scales. At the macroscopic scale cortical and trabecular bone can be distinguished. The cortical or compact bone is located in the outer surface of the bones, is harder, stronger and stiffer than cancellous bone and contributes to the 80% of the weight of human skeleton [37]. The trabecular or cancellous bone is found in the inner part of flat bones, is a highly porous, open-celled structure formed by interconnected plates and needle-like structures (named trabeculae) of bone tissue. The intertrabecular space is filled with marrow containing blood vessels, nerves and several cell types. In long bones the cancellous bone is located at the ends while in short bones or flat bones are located everywhere [37].

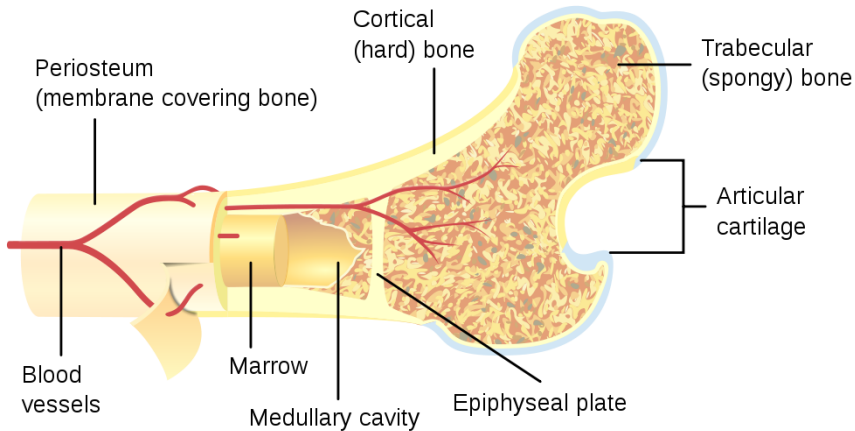


Figure 1.1: *Bone macro-structure of the upper extremity of left femur.* (Reproduced according to the Creative Commons Attribution 3.0 Unported Licence <http://creativecommons.org/licenses/by/3.0/legalcode>)

At a microscopic scale bone has two different structures, lamellar and woven bone. Lamellar bone is formed by concentric parallel layers of crystals and mineralized hardened collagen in a system of short structures known as osteons or Haversian system. This bone is a highly organized, anisotropic, and slowly formed material. The woven bone is a fast formed and poorly organized material in which collagen fibers and crystals are more or less randomly distributed [37]. Most of bone tissue in adult is lamellar, woven bone appearing mainly as a consequence of fracture healing.

Compact Bone & Spongy (Cancellous Bone)

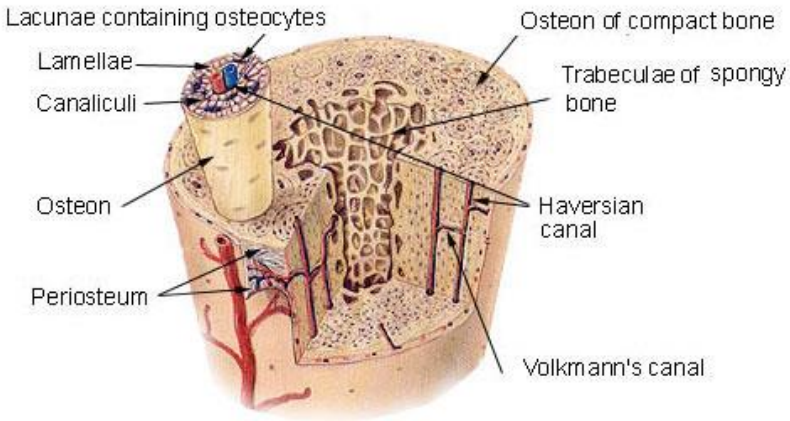


Figure 1.2: *Bone micro structure. Osteons are roughly cylindrical structures that are several millimeters long and around 0.2 mm in diameter [17].* (Reproduced according to the Creative Commons Attribution 3.0 Unported Licence <http://creativecommons.org/licenses/by/3.0/legalcode>)

Several cell types are present in the main stages of bone formation: osteoclasts, osteoblasts, bone lining cells and osteocytes. Bone lining cells, also called pre-osteoblasts or surface osteoblasts, can be found in the periosteal and endosteal surfaces of bones, whereas osteocytes (differentiated osteoblasts) remain trapped in the interior of the mineralized bone forming cavities named lacunae. Osteoblasts, or bone forming cells, are derived from mesenchymal stem cells (as are bone lining cells and osteocytes) and are located in the periosteum. The main product released by osteoblasts is type I collagen, but osteoblasts also secrete other noncollagenous proteins. Osteoblasts form bone by facilitating mineralization but the mechanisms by which this occurs are not well understood [14].

Osteoclasts, or bone resorbing cells, are derived from hematopoietic stem cells. Its main function is to destroy (resorb) mineralized bone and calcified cartilage. An osteoclast is a multinucleated cell, and human osteoclasts on bone have five nuclei and are about 150-200 μm in diameter [22]. (see Figure (1.3))

Bone develops by the process of ossification or osteogenesis. During this process osteoblasts secrete *osteoid*, an amorphous material that gradually becomes densely fibrous. Calcium phosphate crystals are deposited in the osteoid thereby becoming

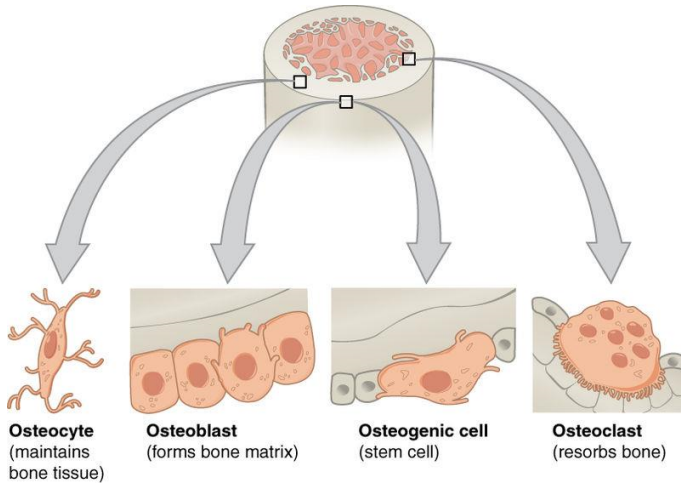


Figure 1.3: *Bone cells that are present in the main stages of bone formation.* (Reproduced according to the Creative Commons Attribution 3.0 Unported Licence <http://creativecommons.org/licenses/by/3.0/legalcode>)

bone matrix. This last part of the process is termed *mineralization*. Two different modes of osteogenesis are observed: intramembranous ossification, in which bone formation occurs directly in primitive highly vascular connective tissue, and endochondral ossification, in which bone formation takes place in pre-existing cartilage. Endochondral ossification occurs in long bone formation (see Figure (1.4)) and in fracture and osteotomy repair [13]. The terms intramembranous and endochondral refers to the type of tissue being replaced, not to the type of bone synthesized, which is the same in both cases [50].

Bone growth and remodelling are two different processes in the skeleton of vertebrates. In the first one bone is formed in sites where it was not present before, results in changes in shape and/or architecture of the bones, and occurs since the first stages of fetal development until the second decade of life in humans [37]. The second process, i.e. replacement of old bone by new one and reparation of microdamage [43], takes place throughout the whole of life and, as we have already remembered, is required for mineral homeostasis, for adapting to mechanical changes and to maintain the healthy functionality of bones.

1.3 Bone remodelling and the Basic Multicellular Units

We have mentioned that bone growth and remodelling are two different processes, a main difference being the destruction of previously existing bone. The replacement of old bone by new one is a process that involves resorption and formation of bone

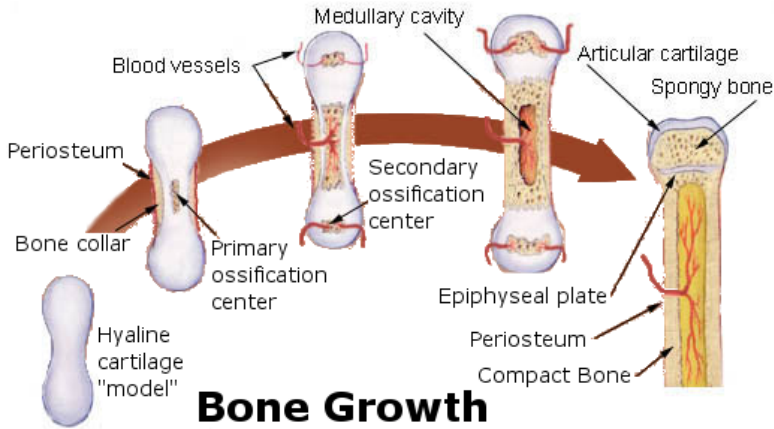


Figure 1.4: *Formation and growth of long bones by endochondral ossification. Mesenchymal condensation leads to a cartilage "model". Chondrocyte undergo apoptotic and cartilage mineralization starts. Vascular invasion from vessels allows the migration of osteoblast precursor cells that deposit bone on the degraded matrix scaffold.* (Reproduced according to the Creative Commons Attribution 3.0 Unported Licence. <http://creativecommons.org/licenses/by/3.0/legalcode>)

without participation of a third tissue (i.e. case of endochondral ossification). Remodelling required for mineral homeostasis need not to occur in specific sites and remodelling related to mechanical changes and damage is site-specific.

The resorption of bone is carried out by osteoclasts acting on small pockets of bone and followed by osteoblasts precursors recruitment that differentiate and replace the resorbed bone by a suitable extracellular matrix (ECM) where bone will be eventually produced. Resorption and formation processes are coordinately carried out by discrete temporaly anatomic units called "Basic Multicellular Units" (**BMUs**) first described by Harold Frost in the sixties [21]. The region where BMU operates, referred to as the bone remodelling compartment (BRC), is a canopy of bone lining cells/osteoblasts and a nearby capillary covering the BMU [49].

BMU are present in cortical and trabecular bone and differ in structure and in the ways they remove and replace bone. In trabecular bone, BMU are located at the surface covered by a canopy of cells of mesenchymal origin. The resorbing zone is cleaned by lining cells and macrophages and osteoblasts precursors differentiate to fill the gap created by osteoclasts. BMU in the cortex display a moving team of osteoclasts in it's front forming the cutting cone or hemicone, the remaining space being filled by blood vessels, nerves and conecting tissue. (see Figure 1.5).

BMU move in three dimensions excavating and refilling a tunnel in cortical bone or a trench across the surface of cancellous bone. A cortical BMU travels about 4000 μm at about 20 $\mu\text{m}/\text{day}$, taking about 200 days to complete it's task. A cancellous BMU travels about half this distance about half the speed, taking about the same period of time to fulfill that process [43]. The resorption period has a duration

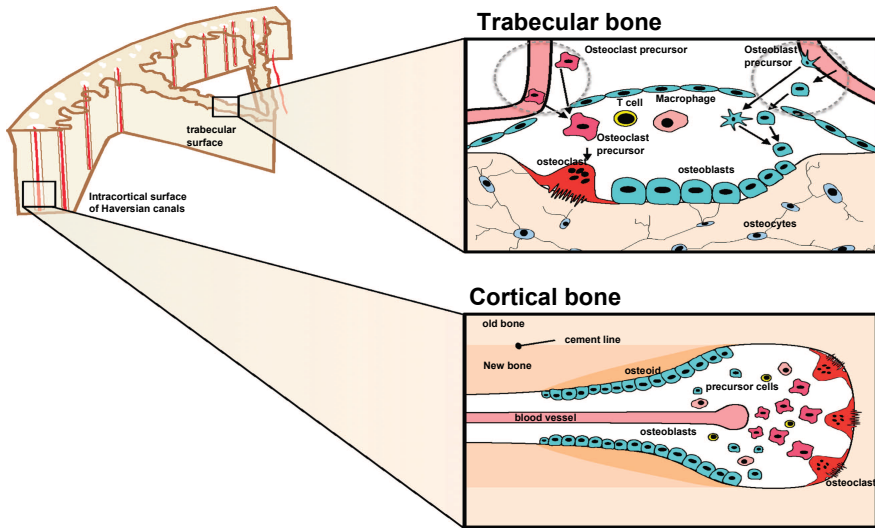


Figure 1.5: *Remodeling is initiated within BRCs at points beneath the canopy of cells lining trabecular bone (upper panels) and within cortical bone Haversian canals (lower panels). Osteoclasts (OCs) are formed from hemopoietic precursors (HSC) supplied by marrow and the bloodstream. Precursors of osteoblasts come from MSCs in the marrow, from blood and from pericytes, and differentiate within the BMU through the osteoblast precursor stage to fully functional synthesizing osteoblasts and to osteocytes; lining cells may also differentiate into active osteoblasts. T cells and macrophages can gain access to the BRC from the blood supply.* (Reprinted by permission from Macmillan Publishers Ltd: BoneKey Reports 3. Article number: 481 (2014) doi:10.1038/bonekey.2013.215, copyright 2014)

between 30-40 days and is followed by the formation period with a mean duration of 150 days [18]. Remodelled regions can be recognized by cement lines that follow the festoon-shaped surfaces that were eroded by osteoclasts [49]. In normal bone, the result of this process is the complete refilling of the resorption lacuna. The successful coordination of bone resorption and formation in each BMU is referred to as coupling (see Figure 1.6). The mechanisms responsible for such coupling remain largely elusive [18]. Any disturbance in coupling may result in pathologies as Osteoporosis, which appears when osteoblasts are not able to fully refill the resorption region, so that a net loss of bone occurs in each remodelling event. Conversely, Osteopetrosis (marble bone disease) results when there is incomplete bone resorption [56].

The key event that triggers the remodelling process is osteocyte programmed cell death or apoptosis, which has been shown to depend on mechanical load [41]. Thus, osteocyte death characterizes the regions under high loading stress that require new bone production, as well as the zones with lower mechanical demand where bone should be removed. In the case of micro-fractures osteocyte death is induced, which leads to subsequent activation of the bone remodelling process. In contrast, in large bone fractures, osteocytes release alert signals that recruit immune cells and can lead to an inflammatory response, thus initiating an alternative pathway of bone

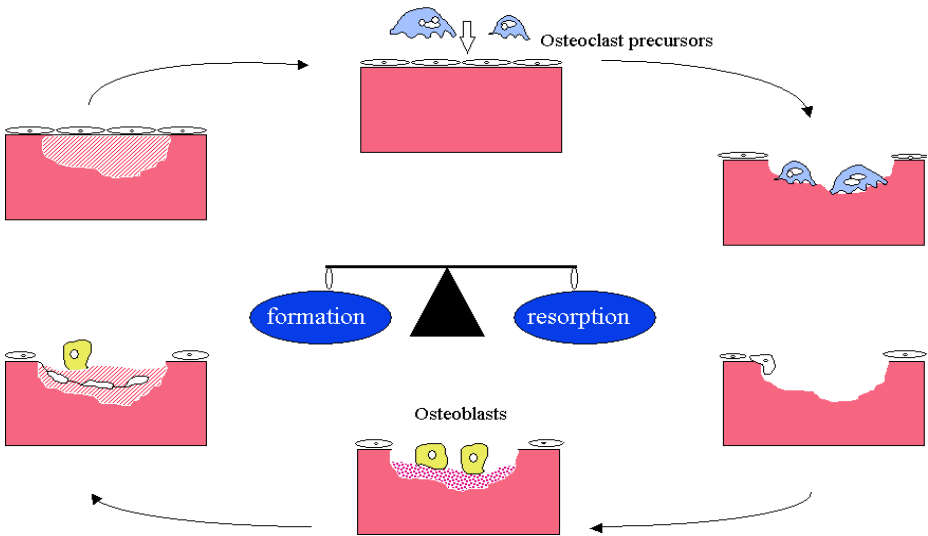


Figure 1.6: *Coupling between bone resorption and formation. The equilibrium between both processes is condition for the repair of microscopical skeletal damage that occurs as a result of constant ground impact. Figure courtesy of Dr. José Manuel Lopez.*

formation that involves other cell types [4].

To this day the mechanisms of cell communication within a BMU remain only partially understood. It's is clear however, that bone remodelling has to be tightly regulated. For instance, an osteoblast should not start secreting osteoid matrix before osteoclasts destruction task is finished. This raises at once the question of how is this coordination achieved, and how could we possibly ascertain the internal circuitry within a BMU that keeps it operative when remodelling is needed, and shuts it off immediately afterwards. Those questions, once being clarified, would help us to understand the coupling between bone resorption and formation. This in turn would greatly extend our current knowledge of bone homeostasis, the strategist to preserve it, and possible methods to restore it when necessary.

1.4 Fracture Healing

The reparation of both bone micro-fractures and larger bone fractures are complex processes that recapitulate aspects of embriological skeletal development [26], but in the case of larger fractures there is a particular sequence of facts that have been well documented. It consists of three overlapping phases termed as inflammatory, reparative and remodelling, each characterized by specific cellular, histological and biochemical features. We next briefly sketch them.

Right after bone breaking the resulting gap is filled with blood. Thrombin gener-

ated by blood vessel disruption induces the cleavage of fibrinogen present in blood to yield fibrin monomers, which actively polymerize afterwards. In this manner a fibrin net is generated that in 6 to 8 hours connects both sides of the fracture, and provides a first scaffold on which bone will be eventually produced [26], [16]. Soon after bone fracture, a number of growth factors (BMP, VEGF, PDGF, ...) are liberated within the fracture gap [5]. Such substances will mediate subsequent steps in bone repair (Figure 1.7, A, B).

As soon as a fibrin clot begins to be formed, new functional blood vessels as well as Mesenchymal Stem Cells (**MSC**) are recruited from the fracture boundaries. **MSC** move in the wake of the new vascular bed created by incoming blood vessels. The latter can be seen within 6 to 12 hours near fracture boundaries, and between 24 to 48 hours they have invaded the whole fracture gap [50].

MSC move inwards from the fracture boundaries, and in doing so they experience both symmetric and asymmetric divisions [36]. Symmetric division, whereby a **MSC** gives raise to two **MSC**, takes place whenever their available initial number is not enough to keep the healing process on time. On the other hand, when a **MSC** reaches the fibrin clot it undergoes asymmetric division, thus giving raise to one **MSC** and to one differentiated cell, whose lineage depends on the density of the net on which division takes place [10], [15], [48]. Cell replication is stimulated by some of the growth factors present, whose action is dependent on the unfolding of the fibrin clot (Figure 1.7 C, D). In particular, anchorage into the net significantly extends the half-life of growth factors with respect to that of freely diffusing ones [53], [9].

Specifically, the first type of asymmetric division takes place over a low-density fibrin clot and gives raise to fibroblasts. Once attached to the net, fibroblasts secrete a number of substances (collagens) which stick to the clot and change its mechanical properties [15], [48]. The resulting network (called fibrous callus) has larger mechanical stability than the earlier fibrin net, although not enough to ensure working stability to the repairing bone (Figure 1.7, E, F, G).

In a period ranging from 48 to 72 hours, the fracture gap is filled with **MSC** and their progenies ([32], [12]), which change as the composition of the net expanding the fracture gap does so. In particular, upon sticking to collagen-enriched fibrin net, **MSC** again undergo asymmetric division that now gives raise to one **MSC** and one chondrocyte ([36], [10]). This new type of cell interacts with the existing net and produces a more stable compound, called cartilaginous callus (Figure 1.7, H, I, J). Bone formation now begins in a subsequent remodelling phase. More precisely, cartilaginous callus is replaced first by trabecular and then by lamellar bone ([53]) through a process similar to endochondral ossification **EO** (Figure 1.7, K, L, M, N).

The micro-fracture healing is of intramembranous type and does not includes an inflammatory phase. In contrast with large fracture, in micro-fracture repair the new bone is formed without resorting to the formation of a fibrin-collagen scaffold and is carried out by the action of the **BMUs**.

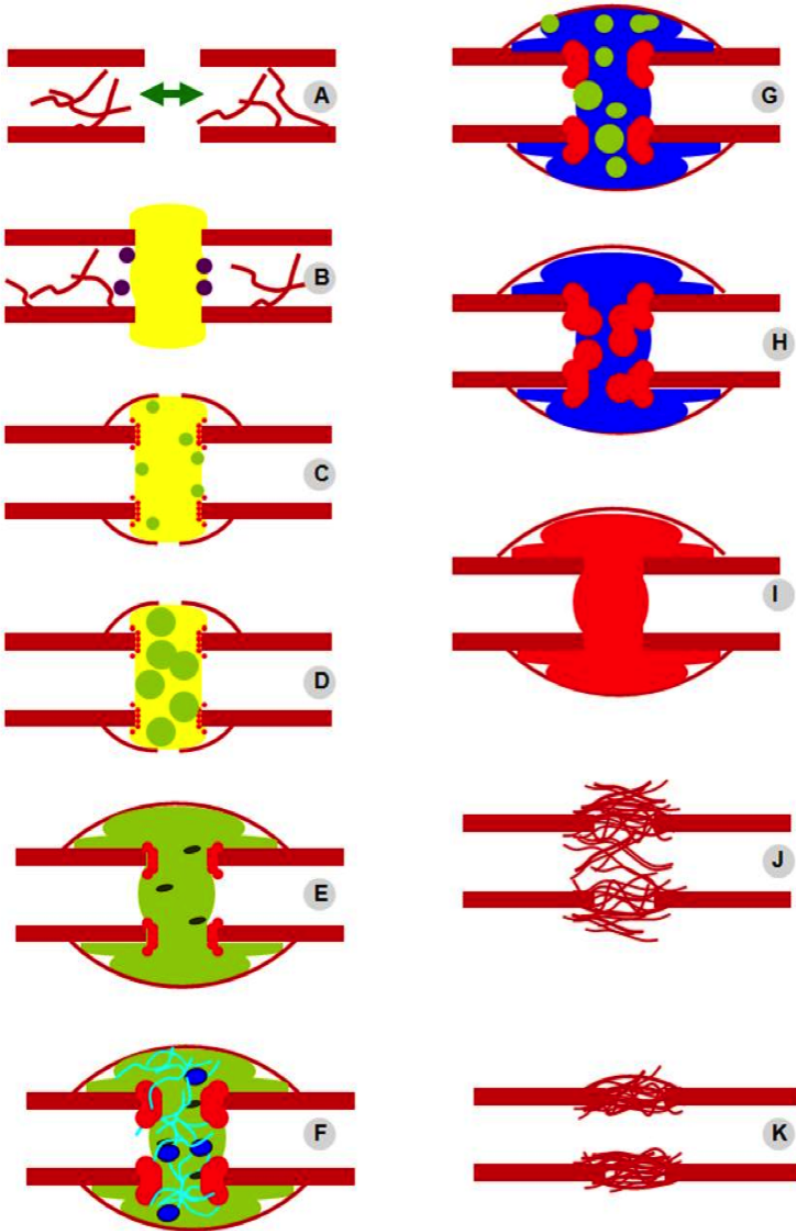


Figure 1.7: Schematic representation of the fracture healing process. It is divided into four stages: the initial inflammatory response (A-B), soft callus formation (C-E), hard callus formation (F-I) and bone remodeling (J-K). Figure courtesy of Dr. José Manuel Lopez

1.5 Mathematical models

As in any other experimental science, what we know about a phenomenon is not the phenomenon itself, but what our understanding, mediated by our language, is able to formulate about the problem studied [33]. In the particular cases of fracture healing and bone remodeling, there are several conceptual models that help us to understand such processes. Some of them will be shortly described below.

Before doing that, a few remarks are in order. To begin with, when deriving mathematical models, two possible (not necessarily conflicting) goals may be pursued. First, one might aim at proposing a set of equations whose solutions should fit a given set of data as closely as possible. One might instead intend that solutions to the model could explain the phenomenon, in that they could be used to make testable predictions that could be falsified by experiments. The first approach looks particularly appealing, and has perhaps been more actively pursued than the second one. However, the history of science has many examples of mathematical models that turned out to be wrong, even though they nicely fit data, which they did by resorting to a large number of equations or to a large number of parameters appearing in them. A particularly well known case is provided by Ptolemy's theory of epicycles introduced to fit planetary motions, and many other examples can be found in different scientific fields, as for instance in theoretical ecology [27]. Such attempts, which showed great ingenuity, often managed to match actual observations. However, they provided no explanation about the actual reasons for the facts observed, so that no real insight on the processes considered was gained for their use.

In this work we shall adopt a different stance, and look for model simplicity as a basic requirement to better understand the phenomena studied. We will thus keep in line with Ockham famous dictum: *among competing hypotheses, that with the fewest assumptions should be selected* [28]. Therefore, in each of the cases addressed we will make explicit a minimal number of assumptions (that will always be biologically motivated) required to explain the process being dealt with. Before doing that, however, a short review of previous models on bone remodeling and fracture repair will be discussed below. For the ease of presentation, such models can be classified in different types as follows.

1.5.1 Mechano-regulatory models

It is widely accepted that mathematical modeling of bone function can be traced back to the pioneering work by Roux [47] and Wolff [55] in the XIX century. In particular, W. Roux hypothesized that the biological processes of bone formation and remodeling are regulated by cell signals generated by mechanical loading, a statement considered as the fundamental premise for mechano-biology [38]. He further proposed that cells within a tissue compete for functional stimulus. On his side, J. Wolff further elaborated the idea that changes in bone structure and shape are a direct consequence of changes on the mechanical stresses acting on bone, a statement that goes (under various versions) under the generic name of Wolff's law. Such general postulate has not remained free of controversy. For instance, according to Cowin [11],

it considers as identical objects that are not so, as for instance stress trajectories in a homogeneous isotropic material and the trabecular structure of cancellous bone. This fact notwithstanding, the assumption of a close link between stress induced and bone structure has remained an inspiring principle in many later studies.

As a matter of fact, the literature on mathematical modeling of bone function and repair has been steadily increasing since the sixties of last century, when the availability of fast and efficient computers allowed for an easier comparison of numerical solutions and experimental data. To classify such models, it has become usual to consider the type of stimuli, mechanical or biological, which is considered as more relevant in each case [25]. Such cases will be respectively termed as mechano-regulatory and bio-regulatory.

Concerning the first type, a breakthrough is usually credited to the work done by Pauwels about 1960 [44]. Based on Roux's ideas, he proposed a theoretical framework according to which mechanical forces acting on tissues determine cell differentiation pathways on such tissues. In particular, he postulated that distortional shear stress is a specific stimulus for the development of collagen fibers, and that hydrostatic compressive stress is a specific stimulus for cartilage formation. According to this author, bone formation requires of a stable, low-strain mechanical environment and endochondral bone formation only occurs after soft tissues have stabilized their environment to that end. Pauwels theory has some limitations though. For instance, no specific stimulus for bone formation is proposed, and his author was not able to measure (or to estimate) in detail actual bone strains or stresses.

Further steps were provided by later models due to Carter et al. [6] and to Claes and Heigele [7]. In these works biological tissues were considered as linear elastic materials, and the formation of bone, cartilage and fibrous cartilage was related to hydrostatic stress and to principal strains. In [6] the case of cyclic mechanical loading was also considered. Different tissue differentiation mechanisms were proposed by Prendergast et al. [45], who considered biological tissues as poroelastic materials and linked differentiation into bone, cartilage or fibrous tissue to differences in fluid flow properties and distortional strains. Subsequently, numerical studies based on the approach proposed in [45] were conducted by Huiskes et al. in [30]. Finally, a fuzzy logic theoretical model was proposed by Ament and Hofer in [1], in which mechanical stimulus was evaluated by means of a strain energy.

A common feature of the works just mentioned is the extensive use of numerical simulations to compare results corresponding to different bone repair situations with experimental data.

1.5.2 Bio-regulatory models

A different approach to bone remodeling was introduced in work by Bailon-Plaza and van der Meulen [2]. These authors proposed a mathematical model where the effect of chemical cues, particularly growth factors, in bone remodeling was introduced. Ever since, models where chemical signals are the most relevant players retained are customarily termed as bio-regulatory. In [2], the action of growth factors on intramembranous and endochondral ossification was discussed. To do that,

authors formulated a PDE system involving seven variables, namely the densities of mesenchymal stem cells (MSCs), osteoblasts and chondrocytes, concentrations of chondrogenic and osteogenic growth factors, and densities of connective/cartilage extracellular matrix (ECM) and bone ECM. Authors considered processes as cell differentiation, proliferation, migration and death, as well as synthesis and resorption (destruction) of bone tissue. A number of interesting conclusions about the regulatory role played by growth factors in bone healing were drawn from the numerical simulations performed.

In 2008, Geris et al. presented in [24] a model based on previous work in [23] which includes additional features as the impact of angiogenesis (that is, the recruitment of new vessels from a pre-existing vasculature) on bone repair. To that end, additional variables were introduced to those already considered in [23]: density of endothelial cells, fibroblasts concentration, vascular matrix and fibrous tissue densities as well as a generic angiogenic growth factor. In that way a model was arrived at containing 12 variables in a similar number of coupled PDEs with 73 parameters in all.

The cases considered in our two previous paragraphs focused mainly on mechanical or biological regulation of ossification and bone repair. It is natural to consider the possibility of integrating both approaches, thus leading to what are known as *mechano-bio-regulatory models*. A significant step in this direction was provided by Bailon-Plaza and van der Meulen in [3]. Building on their previous work [2], they presented there a framework which specifically incorporates the effect of mechanical stimulus on cell activity. This approach, which naturally results in increasing levels of model complexity, has been later pursued by many authors (see for instance [39], [46]). Besides there are models for bone remodelling that represent remodeling on the scale of an individual basic multicellular unit (BMU) (see [35], [35]), and models that extending the later ones, include the osteocyte population to acomodate the effects of mechanical loading [40]. However, we shall refrain from adding further details here since we intend to explore a different approach in this memoir. Instead, further relevant information of previous work will be provided in the following chapters where adequate.

It follows from our previous remarks that the quest for comprehensive models, where all biological process known to date are included , necessarily leads to large systems of equations with an even larger number of parameters (representing reaction rates, diffusion coefficients, etc) which are basically unknown. It is natural to select them so that a particular experiment could be satisfactorily fitted. However, most often the values thus obtained should be changed if a different experiment is considered, and in general little insight can be gained in this manner about the internal logic of the process under consideration. As we have already mentioned, one could however try a different approach, and look instead for the minimal set of biological ingredients that have to be retained in a model so that it can reproduce what is actually observed. See for instance [19] for an example of a bio-regulatory model in this vein. See also [29] for a survey of mathematical techniques to deal with bio-regulatory models.

Bibliography

- [1] Ament, C. & Hofer, E. P. 2000 *A fuzzy logic model of fracture healing*, Journal of Biomechanics, **33**, (2000), 961-968. (doi:10.1016/S0021-9290(00)00049-X)
- [2] Bailon-Plaza, A. & van der Meulen, M. C. H. 2001 *A Mathematical framework to study the effects of growth factor influences on fracture healing*, Journal of Theoretical Biology., **212**, (2001), 191-209. (doi:10.1006/jtbi.2001.2372)
- [3] Bailon-Plaza, A. & van der Meulen, M. C. H. 2003 *Beneficial effects of moderate, early loading and adverse effects of delayed or excessive loading on bone healing*, Journal of Biomechanics., **36**, (2003), 1069-1077. (doi:10.1016/S0021-9290(03)00117-9)
- [4] J.P. Bidwell, J. Yang & A. G. Robling 2008. *Is HMGB1 an osteocyte alarmin?*. J. Cell. Biochem. **103/6** 1671-1680.
- [5] Bolander, M.E. 1992. *Regulation of fracture repair by growth factors*. Proc Soc Exp Biol Med. **200**, 165-170.
- [6] Carter, D. R., Blenman, P. R. & Beaupre, G. S. 1988 *Correlations between mechanical stress history and tissue differentiation in initial fracture healing.*, J. Orthop. Res., **6**, 736-748. (doi:10.1002/jor.1100060517)
- [7] Claes, L., Wilke, H.-J., Augat, P., Rubenacker, S., & Margevicius, K., 1995 *Effect of dynamization of gap healing of diaphyseal fractures under external fixation*, Clinical Biomechanics ., **8**, (1995), 227-234.
- [8] Claes, L. E. & Heigele, C. A. 1999 *Magnitudes of local stress and strain along bony surfaces predict the course and type of fracture healing*, Journal of Biomechanics., **32**, (1999), 255-266. (doi:10.1016/S00219290(98)00153-5)
- [9] Cole, A.A., & Walters, L.M. 1987. *Tartrate-resistant acid phosphatase in bone and cartilage following decalcification and cold-embedding in plastic*. J. Histochem. Cytochem. **35**, 203-206.

- [10] Colnot, C., Huang, S., Helms, J. 2006. *Analyzing the cellular contribution of bone marrow to fracture healing using bone marrow transplantation in mice*. *Biochem. Biophys Res Commun*, **350**, 557-561
- [11] Cowin, S. 2001. *The false premise of Wolff's law*. In: Cowin, S.C. (Ed.), *Bone Biomechanics Handbook*. CRC-Press, Boca Raton, pp. 1?14 (Chapter 30).
- [12] Deckers, M.M.L., van Bezooijen, R.L., van der Horst, G., Hoogendam, J., van der Bent, C., Papapoulos, S.E. et al. 2002. *Bone morphogenetic proteins stimulate angiogenesis through osteoblast-derived vascular endothelial growth factor A*. *Endocrinology*, **143**, 1545-1553.
- [13] Doll, B. 2005 *Developmental Biology in the Skeleton system*. In *Bone Tissue Engineering*. Edited by Hollinger, J., Einhorn, T. Doll, B. & Sfeir, C. CRC Press.
- [14] Donahue, H. J., Siedlecky, C. A. & Vogler, E. 2005 *Osteoblastic and Osteocytic Biology in Bone Tissue Engineering*. In *Bone Tissue Engineering*. Edited by Hollinger, J., Einhorn, T. Doll, B. & Sfeir, C. CRC Press.
- [15] Eghbali-Fatourehchi, J., Lamsam, D., Fraser, D., Nagel, B.L., Riggs, S. & Khosla 2005. *Circulating osteoblast-lineage cells in humans*. *N Engl J Med*. **352**, 1959-1966.
- [16] Einhorn, T.A. 1998. *The cell and molecular biology of fracture Healing*. *Clin.Orthop.Relat. Res* **355**, S7-21.
- [17] Encyclopaedia Britannica (Online). Documenting electronic sources on the internet. (Date of consult: october 2014). Available in: <http://global.britannica.com/EBchecked/topic/434325/osteon>
- [18] Erik Fink Eriksen 2010 *Cellular mechanisms of bone remodelling* *Rev Endocr Metab Disor* **11** 219-227
- [19] Fasano, A. Herrero, M., Lopez, J.M., & Medina, E. 2010 *On the dynamics of the growth plate in primary ossification*. *J. Theor. Biol.* **265** 543-553.
- [20] Ferguson, C., Miclau, T., Alpern, E. & Helms, J. 1999 *Does adult fracture repair recapitulate embrionic skeletal formation?* *Mech. Dev.* **87** 57-66
- [21] Frost H. M. 1964 *Dynamics of bone remodelling*. *Bone Biodyn.* 315-333. (Book Chapter)
- [22] Gay, C.V. 2005 *The osteoclast* In *Bone Tissue Engineering*. Edited by Hollinger, J., Einhorn, T. Doll, B. & Sfeir, C. CRC Press.
- [23] Geris, L. Gerisch, A., Maes, C., Carmeliet, G., Weiner, R., Van Oosterwyck, H., & Vander Sloten. 2006 *Mathematical model of fracture healing in mice: comparison between experimental data and numerical simulations*. *Med Biol Eng Comput* **44**, 280-289. (doi:10.1007/s11517-006-0040-6)

- [24] Geris, L., Gerisch, A., Vander Sloten, J., Weiner, R. & Van Oosterwyck, H. 2008 *Angiogenesis in bone fracture healing: a bioregulatory model*. Journal of Theoretical Biology **251**, 137-158. (doi:10.1016/j.jtbi.2007.11.008)
- [25] Geris, L., Vander Sloten, J., & Van Oosterwyck, H. 2009 *In silico biology of bone modelling and remodelling*, Philosophical Transactions of the Royal Society., **367**, (2009), 2031-2053. (doi:10.1098/rsta.2008.0293)
- [26] Gerstenfeld, L.C., Cullinane, D.M., Barnes, G.L., Graves, D.T., & Einhorn, T.A. 2003. *Fracture healing as a post-natal developmental process: molecular, spatial, and temporal aspects of its regulation*. J Cell Biochem. **88**, 873-884.
- [27] Ginzburg, L. R. & Jensen, C. X. J. *Rules of thumb for judging ecological theories*. Trends in Ecology and Evolution. **19/3** 121-126
- [28] Hamilton, Sir William. 1860. *Lectures on Metaphysics and Logic*. Oxford University Press.
- [29] Herrero, M. & Lopez, J.M. 2005 *Bone formation: biological aspects and modeling problems*. Theor. Med. **6/1** 41-55.
- [30] Huiskes, R., van Driel, W.D., Prendergast, P.J., & Soballe, K. 1997. *A biomechanical regulatory model for periprosthetic fibrous-tissue differentiation*. J. Mater. Sci. Mater. Med. **8** 785-788. (doi:10.1023/A:1018520914512)
- [31] Huiskes, R. 2000 *If bone is the answer, what is the question?*. J. Anat. **197**. 145-156.
- [32] Kalfas, I.H. 2001. *Principles of bone healing*. Neurosurg Focus, **10**.
- [33] Kant, I. 1788. *Critique of Pure Reason*. Translated into english by Norman Kemp Smith 1929. Cambridge University Press.
- [34] Komarova, S., Smith, R., Dixon, S., Sims, S., & Wall, L. 2003 *Mathematical model predicts a critical role for osteoclast autocrine regulation in the control of bone remodelling*. Bone **33** 225-234.
- [35] Komarova, S. 2005 *Mathematical model of paracrine interactions between osteoclasts and osteoblasts predicts anabolic action on parathyroid hormone on bone*. J. Endocrinol. **146** 3589-3595
- [36] Malizos, N. & Papatheodorou, L.K. 2005. *The healing potential of the periosteum. Molecular aspects*. Injury **36** (Suppl 3), S13-S19.
- [37] Marks, S. C. & Odgren, P. R. 2002. *Structure and development of the skeleton*. In Principles of Bone Biology 2 ed. Edited by Bilezikian, J. Raisz, L. & Rodan, G. Academic Press.
- [38] van der Meulen, M.C., & Huiskes, R., 2002 *Why mechanobiology ? A survey article* J. Biomech. **35** 401-414.

- [39] Moreo, P., Garcia Aznar, J., Doblare, M. 2009. *Bone ingrowth on the surface of endosseous implants. part i: mathematical model*. J. Theor. Biol **260**, 1–12 (2009)
- [40] Moroz, A., Crane, M., Smith, G., & Wimpenny, D. *Phenomenological model of bone remodelling cycle containing osteocytes regulation loop*. Biosystems. **84** 183-190.
- [41] B.S. Noble, N. Peet, H.Y. Stevens, A. Brabbs et al. 2003. *Mechanical loading : biphasic osteocyte survival and targeting of osteoclasts for bone destruction in rat cortical bone*. Am. J. Phys-Cell Phys. **284/4** C934-C943.
- [42] Overgaard, S. 2000 *Calcium phosphatae coatings for fixation of bone implants.*, Acta Orthopaedica Escandinavica Supplementum, **297**, (2000), 1-74. (doi:10.1080/000164700753759574)
- [43] Parfitt, A. M. 2002 *Targeted and not targeted bone remodelling: Relationship to basic multicellular unit origination and progression*. Bone **30/1**, 5-7.
- [44] Pauwels, F. 1960 *Eine neue Theorie uber den Einfluss mechanischer Reize auf die Differenzierung der Stutzgewebe*. Z. Anat. Entwicklungsgeschichte **121**, 478-515. (doi:10.1007/BF00523401)
- [45] Prendergast, P. J., Huiskes, R. & Soballe, K. 1997 *Biophysical stimuli on cells during tissue differentiation at implant interfaces.*, J. Biomech. **30** 539-548. (doi:10.1016/S0021-9290(96)00140-6)
- [46] Prokharau, P. Vermolen, F. & Garcia-Aznar, J. M. 2012 *Model for direct bone apposition on pre-existing surfaces, during peri-implant osseointegration.*, Journal of Theoretical Biology., **304**, (2012), 131-142.
- [47] Roux, W. 1881 *Der Kampf der Teile im Organismus: ein Beitrag zur Vervollstandigung der mechanischen Zweckmassigkeitslehre*. Engelmann, Leipzig.
- [48] Rumi, M.N., Deol, G.S., Singapuri, K.P., & Pellegrini Jr. V.D. 2005. *The origin of osteo- progenitor cells responsible for heterotopic ossification following hip surgery: an animal model in the Rabbit*. J Orthop Res. **23**, 34-40.
- [49] Sims, N. & Martin, T. J. 2014 *Coupling the activities of bone formation and resorption: a multitude of signals within the basic multicellular unit*. BoneKEy Reports **3**, Article Number 481. 1-10.
- [50] Shapiro, F. 2008 *Bone development and its relation to fracture repair: The role of mesenchymal osteoblasts and surface osteoblasts*. European Cells and Materials. **15** 56-73.
- [51] Steiniche, T., & Hauge, E. M. 2003 *Normal structure and function of bone*. In Handbook of Histology for Bone and cartilage. Humana Press. New Jersey.

- [52] Strom, O. Borgstrom, F., Kanis, J. A. Compston, J. Cooper, C. McCloskey, E. V. & Johnsson, B. 2011. *Osteoporosis: burden, health care provision and opportunities in the European Union*. Arch Osteoporos. **6**. 59-155 DOI 10.1007/s11657-011-0060-1.
- [53] Takahara, M., Naruse, T., Takagi, M., Orui, H., & Ogino, T. 2004. *Matrix metalloproteinase-9 expression, tartrate-resistant acid phosphatase activity, and DNA fragmentation in vascular and cellular invasion into cartilage preceding primary endochondral ossification in long bones*. J Orthop Res. **22**, 1050-1057.
- [54] U.S. Department of Health and Human Services 2004. *Bone Health and osteoporosis: A Report of the Surgeon General*. Available at: <http://www.ncbi.nlm.nih.gov/books/NBK45513/> .
- [55] Wolf, J. 1892. *Das Gesetz der Transformation der Knochen*. Verlag von August. Berlin. Translated as: *The Law of bone remodelling*. Springer Verlag. Berlin, 1986.
- [56] Zaidi, M. 2007 *Skeletal remodelling in health and disease*. Nature Medicine. **13/7** 791-801

Bone remodelling

2.1 Introduction

It is well known that bone microscopic structure continuously adapt to meet the resulting mechanical requirements. This adaptation is achieved by means of a bone remodeling process that is maintained throughout life, and whose control relies on osteocytes, the most abundant cell type in bone [1, 2].

Osteocytes act as mechanosensors that monitor mechanical stress within bone tissues, reacting to changes in both the amount and the direction of loading on bone and ensuring that remodeling only takes place where needed. The key event that triggers the remodeling process is osteocyte programmed cell death or apoptosis, which has been shown to depend on mechanical load. The relation between osteocyte apoptosis and load applied is U-shaped, i.e., mechanical stresses within a normal physiological range prevent it, whereas those above or below this range favor it [3, 4, 5]. Thus, osteocyte apoptosis is a marker both for regions under high loading stress that require new bone production, and for zones with lower mechanical demand where bone should be removed. Micro-fractures, which are continuously being produced as a consequence of physical exercise in healthy individuals, also result in osteocyte apoptosis and subsequent activation of the bone remodeling process. In bone fractures, a considerable amount of osteocytes are compromised and alert signals are produced that recruit immune cells and lead to an inflammatory response. In this manner an alternative pathway of bone formation is started where other cell types are involved [6]. We shall not deal with this second situation here, since we will be concerned with homeostatic bone remodeling at comparatively smaller scales. The way in which this process is carried out is now discussed below.

Once triggered by osteocyte apoptosis, a bone remodeling process is executed by organic teams called Basic Multicellular Units (BMU) [7]. Each BMU consists of several morphologically and functionally different cell types (mainly osteocytes, osteoblasts and osteoclasts) that act co-ordinately in small cavities, called Bone re-

modeling Compartments (BRC) where remodeling takes place [8, 9]. The behaviours of the different cell types involved can be summarized as follows. A normal presence of osteocytes keeps osteoblasts deactivated and precludes osteoclast precursors from being recruited. When a group of osteocytes undergoes apoptosis, a drop in inhibitory action results that has several consequences. In particular, it leads to osteoblasts activation and to the attraction of osteoclast precursors arising from the bone marrow. These precursors subsequently differentiate into mature osteoclasts, which start destroying surrounding bone, leading to the appearance of the so-called cutting cones [10]. In a later stage of the process, activated osteoblasts, marching in the wake of bone-destroying osteoclasts, will replenish the cavity left behind the latter with an osteoid matrix. Some of the active osteoblasts remain trapped in the bone matrix and differentiate into osteocytes [11], which in turn will be instrumental in the subsequent mineralization of the matrix surrounding them, thus concluding local bone remodeling. The whole process is summarized in Figure 1.

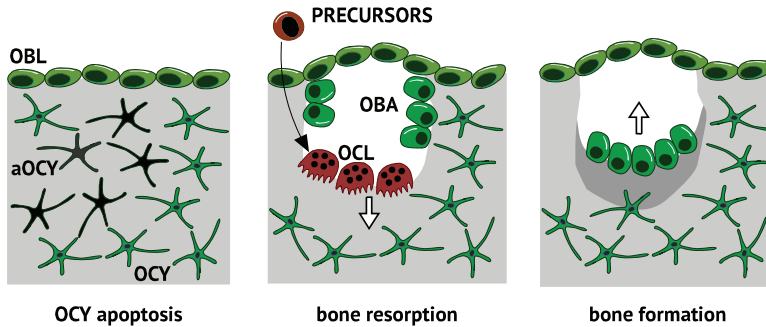


Figure 2.1: **A sketch of BMU operation after a group of osteocytes has undergone apoptosis near bone surface.** Left) Bone interior (in gray) contains a number of functional osteocytes (OCY, in green). Apoptotic osteocytes (aOCY, in black) cease to release osteoblasts (OBL) inhibitors, which in particular leads to the activation of OBL placed at the bone surface. Center) A remodeling process starts. As a further consequence of the drop in OCY-induced inhibitory effects, Osteoclast precursors are recruited and differentiate into active osteoclasts (OCL, in red). OCL then form cutting cones that start the destruction (resorption) of surrounding bone. Later on, activated osteoblasts (OBA) move inwards in the trail open by OCL. Right). When the bone-remodeling compartment (BRC) reaches a large enough size, OCL die by apoptosis and OBA secrete osteoid matrix. OBA then differentiate into OCY and remain trapped in that matrix, which is eventually mineralized, thus completing the formation of new bone.

The process just recalled is exquisitely regulated. For instance, in addition to taking place only where is needed, the amount of new bone generated should equal that of old bone destroyed. Achieving such a balance requires of a coordinated action of all cell types involved. To this day, and in spite of substantial progress achieved

during the last 50 years, the mechanisms of cell communication within a BMU remain only partially understood. It is known however that such regulation is of a local nature since remodeling, which is continuously taking place, is simultaneously and independently occurring in different parts of the skeleton [12]. The process under consideration is a consequence of individual cell decisions. In fact, at any place where the process is going on, individual cells within a BMU are not aware of the pace at which remodeling is proceeding. Nevertheless, to efficiently fulfill its function, any such cell should perform its task according to a precise schedule. For instance, an osteoblast should not start secreting osteoid matrix before osteoclasts destruction task is finished. This naturally raises the question of how is this timing achieved, and what internal circuitry within a BMU keeps such unit operative when remodeling is needed, and shuts it off immediately afterwards. We shall address these issues in the following sections.

Specifically, in this work we formulate and analyze a simple, space-dependent mathematical model that is able to describe BMU operation. Simplicity is here a key issue. We assume that any cell type within a BMU can only take a very limited number of actions (divide, die, differentiate) each being blocked within that cell by a specific inhibitor molecule. The internal dynamics of such inhibitors is coupled with the external medium via a minimal number of cell-to-cell signaling cues, which upon binding with membrane receptors act as sources or sinks for the internal inhibitors. The first of them which falls below a threshold value determines a decision within the previous list in each cell. We will show that only three signaling molecules, acting on cells that can select one between at most three options, are enough to keep a BMU fully operational. Other than choosing a given cell fate over another, cells in a BMU move in response to environmental signals. For instance, osteoclasts form cutting cones by moving inwards into the bone to be resorpted. On the other hand, active osteoblasts lying behind cutting cones will eventually move in the opposite direction during bone formation stage. This dynamic aspect of BMU operation will also be included in our mathematical model.

Once our approach has been stated, a few remarks are in order. To begin with, one may wonder how three signaling cues can possibly be enough for our purposes, taking into account that a much larger set of mediating molecules have been described in the context of bone remodeling (some of them will be recalled below for convenience of the reader). We believe that this is related to some features of the signaling network involved that are far from being fully understood as yet. Namely, we refer to multi-functionality (the fact that a given signal may induce quite different effects in different cell types) and redundancy (the presence of several molecules that may produce the same effect in a given cell type). We do not aim here at providing a priority list between the signals described. What we show instead is that three such cues are enough to regulate the internal inhibitors of the cells considered, so that BMU operation results as an emergent property of the individual decisions taken by any cell involved. Interestingly, such inhibitors have been described in the literature, and the actions induced by the signals proposed have been associated to various of the molecules identified in bone remodeling. We shall provide additional

details on these topics in our next section.

A consequence of the previous remarks is that we do not aim at providing a comprehensive model of bone remodeling where most (if not all) possibly involved processes are retained, but rather at identifying the minimal BMU software required to keep such unit operative. We believe that this may be a useful complement to previous mathematical models available (see for instance [13, 14, 15] and references therein). In these works, great attention is paid to include as many biological data as possible in the models considered, which in particular leads to difficult problems related to actual parameter fitting for the processes involved. In spite of such obstacles, and as a consequence of authors ingenuity, quite interesting results have been obtained in such (and other) references. We hope that a combined use of both approaches (comprehensive and minimality -driven) could shed further light into our understanding of bone remodeling , and particularly on its control when such type of action would be required .

We conclude this introduction by describing the plan of this work. We first recall in Section 2.2 below some known results about cell types involved in BMU functioning, their internal inhibitors and some of the main chemical signals that have been described to mediate bone remodeling. In Section 2.3 we then formulate our mathematical model which is subsequently simulated in Section 2.4 to yield a number of results. In particular, we discuss there the manner in which the number of cells in a BMU is determined by the BRC size, describe how osteoclast lifespan depends on the depth of the BRC and show that the BMU circuit proposed is robust to external noise. The paper then concludes with a Section 2.5, where our results are discussed and possible future directions are shortly described.

2.2 A minimal software for BMU operation

In this section we shall briefly recall some of the chemical signals that are known to be involved in bone remodeling by BMUs. Specifically, a list will be provided of the main molecular mediators in BMU operation currently known, and of the effects they induce in the different cell types involved. In-depth reviews can be found, for instance, in [8, 16, 17, 12].

2.2.1 The role of molecular signals in bone remodeling

A considerable number of chemical signals involved in BMU actions have already been identified. For instance, sclerostin is secreted by normal osteocytes and is known to inhibit both osteoblast activation and osteoclast recruitment from precursor cells in the bone marrow [8, 18]. This inhibitory effect prevents the activation of BMUs in regions where bone remodeling is not needed. In fact, only when a sufficient number of osteocytes undergo apoptosis in a given area, due for instance to micro-fractures or changes in mechanical load, will the inhibitory effect of sclerostin be removed, thus entailing the activation of a BMU and the subsequent initiation of a bone remodeling event.

A set of signals known under the generic name of Bone Morphogenetic Proteins (BMPs) have been described to play a key role during the first stages of bone remodeling. Some members of this family, such as TGF- β and TGF- α , are known to foster differentiation of mesenchymal stem cells to osteoblasts [19, 20]. TGF- β can also induce migration of osteoblasts to the sites of bone formation during remodeling [21] and inhibits osteoblast apoptosis [4]. TGF- β is mainly produced by osteocytes [18, 22], but it is also present in the bone matrix [19] and in platelets [23]. This last factor, together with other signals such as HMGB-1 [6] provide a link with inflammatory processes occurring at early stages of larger fractures repair. Cytokines such as IGF-1, released from bone matrix, seem to play a similar role in activating osteoblast differentiation [21] and are necessary for their survival in vitro [24].

The next stage in the process consists in the recruitment of osteoclasts to the site of bone remodeling. The main signals involved in this step are M-CSF and RANKL [25, 26, 17], that promote the differentiation of osteoclast precursors and the survival of activated osteoclasts. Since RANKL is mostly produced by activated osteoblasts [8, 25], osteoclasts will only be recruited to sites where bone remodeling has already been triggered. Furthermore, in case of a contingent activation of osteoclast precursors where bone remodeling is not necessary, osteoclasts will die by apoptosis in the absence of activated osteoblasts nearby. This provides a security mechanism that avoids the presence of active osteoclasts out of the context of BMU operation. The release by inactive osteoblasts and osteocytes of osteoprotegerin (OPG), a molecule that inhibits the action of RANKL on osteoclasts [25, 26, 27], can also be understood as a checkpoint mechanism that ensures that osteoclasts will only be activated and kept alive in the presence of a sufficient number of activated osteoblasts. Besides inhibiting osteoblast activation, sclerostin also induces apoptosis of active osteoclasts [8, 18]. It may thus act as a signal that stops bone resorption when the cutting edge has reached the required depth in each remodeling event. Finally, osteoid matrix production by active osteoblasts, as well as differentiation of osteoblasts into osteocytes seem to be cell-density dependent [28], and have been suggested to be mediated by connexin, a molecule that circulates through gap junction communications between osteoblasts, as well as by sclerostin [16, 29].

Concerning signalling effects, one also has to bear in mind that: I) different signals can have redundant effects; for example both TGF- β and IGF-1 induce osteoblast differentiation [21], II) a same signal can have different, even opposite, effects on different cell types. For instance TGF- β , FGF and PDGF activate osteoblast and inhibit osteoclast action [23] and G-CSF is known to induce apoptosis and to inhibit differentiation in osteoblasts [26], and III) signals are not always provided by chemicals. In this context we have already remarked that osteocytes act as sensors that respond to changes in mechanical stress in bone [27, 31].

The list just provided of molecular mediators and their effects on BMU cell types, which is summarized in Table 1 below, is far from being complete. Moreover, knowing the identity of molecular mediators or describing their effects in qualitative terms is not enough to explain BMU operation during bone remodeling. In order to understand how a coherent collective plan of action emerges at a multicellular

scale, it is also necessary to take into account quantitative aspects of the process. Indeed, for any given set of signals involved, the amount of bone to be resorpted and produced in different remodeling events can be highly variable [8]. This implies in turn that the number and activity of cells recruited in a BMU should change to suit the needs of each particular remodeling process [22, 23, 30, 32]. Notice also that the references quoted do not focus on quantitative aspects of the process, such as the rate of the production of signals by BMU cell types, or their effect at different concentrations.

Signal	Source	OCL	OBL	OBA
HMGB-1	aOCY	Recruitment Chemotaxis	Recruitment Chemotaxis	Chemotaxis
RANK, OPG M-CSF	OBA aOCY	Recruitment Activation Survival	-	-
Sclerostin	OCY	Inhibition	No proliferation No differentiation Apoptosis	No proliferation No differentiation Apoptosis
TGF- β BMPs PDGF IGF FGF	OCY OBL OBA	Inhibition	Chemotaxis Recruitment Differentiation Proliferation Survival	Chemotaxis Differentiation Proliferation Survival

Table 2.1: A brief summary of the main signals involved in BMU operation as described in the literature (see references in the text)

In our view, the key to understand BMU operation is signal integration by individual cells, as discussed in the next section.

2.2.2 Signal integration by individual cells. Inhibitory proteins

We now postulate our basic modelling assumptions, which can be summarized as follows. Cells within a BMU integrate the molecular signals in their immediate surroundings and, based on the information conveyed by these signals, they chose one among a very limited set of actions, namely differentiation, cell division, migration and apoptosis. In addition, we postulate that inhibitory proteins, that block the progression of these actions within each cell type, mediate cell decisions in any bone-remodeling event.

This last assumption is illustrated by the well-known behaviour of two inhibitory proteins, Rb and Bcl-2. The retinoblastoma protein (Rb) arrests progression into the cell cycle, whereas the B-cell lymphome-2 protein (Bcl-2) precludes the initiation of the apoptosis program in most cell types, including osteocytes and other stromal cells [27]. More precisely, Rb binds to transcription factors of the E2F family, preventing

the progression of the cell cycle to the synthesis stage [33]. When the amount of active Rb falls below a critical threshold, a no-return point is reached (the Restriction Point of the cell cycle) that irreversibly leads to cell division. Analogously, Bcl-2 precludes the release of cytochrome c through the mitochondrial outer membrane, thus avoiding the initiation of the apoptosis program. If Bcl-2 is depleted beneath a suitable value, its inhibitory action is lost and the cell is committed to die [34, 23]. Hence a competition between inhibitory molecules results in a mechanism of cell fate control: the first of these inhibitors (Rb or Bcl-2) that falls below its corresponding threshold value determines the cell decision to divide or die and, importantly, the timing of such decision (see Figure 2.A). This mechanism also provides an explicit link between external signals and cell decisions, given that membrane receptors are known to modulate the evolution of inhibitory molecules within the cell [34]. As a matter of fact, it has been recently shown that the interplay between receptor/signal interaction and the internal dynamics of Rb and Bcl-2 suffices to explain the onset of emergent population properties (as clonal expansion and contraction) in the case of immune response to acute infections [35].

We suggest that a similar approach can be implemented to unravel a BMU operational mechanism. For instance, the existence of inhibitory proteins controlling cellular processes during bone remodeling is well documented in the literature. In fact, two restriction points have been identified in the differentiation program of osteoblasts (marking respectively the transition to activated osteoblast and osteocyte types) that lead to the arrest of the process in the absence of the right signals [23]. One of these restriction points is determined by the inhibition of the transcription factor Runx2 [36] by the action of proteins of the Twist family [37]. Moreover, TGF- α and BMP signalling are known to mediate Runx2 dynamics, thus modulating osteoblast differentiation [38, 39, 40]. The increased complexity derived from the presence of more than one cell type, together with the existence of several cell fates (division, apoptosis or alternative differentiation programs) now introduces new possibilities with respect to the basic dichotomy cell division vs. cell death considered in [35]. However, the underlying logic can be extended to account for these new alternatives. For instance, several inhibitory molecules can simultaneously block the progression of alternative differentiation programs. In this case, the first inhibitor to reach its critical threshold will unambiguously determine the fate of the cell (see Figure 2.B). We postulate that cell choices thus determined are mutually exclusive. This seems to be the case for BMU cells. For instance, osteoblasts that start the differentiation program or decide to secrete osteoid matrix do not complete the cell cycle, and therefore do not proliferate [23]. We also remark that this mechanism allows for one signal to induce alternative cell decisions depending on its concentration.

2.3 Mathematical modelling

Bearing in mind the multiplicity of signals recalled in Table 2.1, as well as the redundancy often observed in their functioning, we propose that the effective operation of a BMU can be modelled by means of a reduced version of the complex signalling

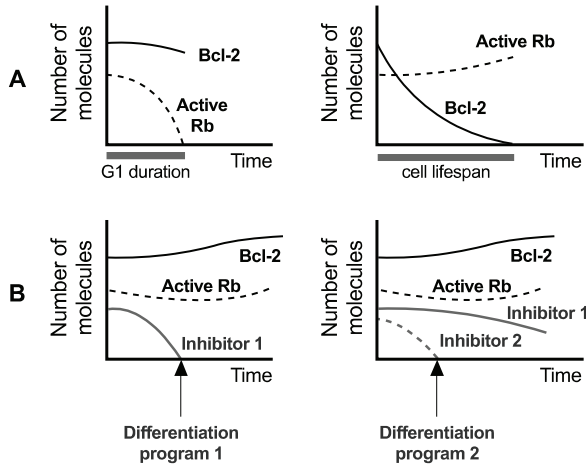


Figure 2.2: **A mechanism of cell fate determination. A)** Inhibitory proteins Rb and Bcl-2 provide a fate decision mechanism in several cell types. The first of these molecules to reach its critical threshold determines if the cell will divide or undergo apoptosis. For convenience all inhibitory thresholds are set equal to zero. **B)** The presence of inhibitors blocking alternative differentiation programs allows to increase the complexity of this cell fate-decision mechanism. **B Left)** If differentiation is assumed to be blocked by Inhibitor 1, which happens to vanish before Rb and Bcl-2 do, then the cell will not divide or die, but will instead undergo differentiation program 1. **B Right)** Two alternative differentiation programs can be controlled by two different inhibitors (1 and 2). If one of them (inhibitor 2 in this case) disappears faster than the remaining molecules, the corresponding differentiation program is selected.

network previously described. Specifically, we propose that three cell-released signals, denoted by R, S and T suffice for that purpose. The effect induced by such signals in the cell types involved is described in Table 2.2 We will next describe the main ingredients of the model proposed in this work.

2.3.1 Cell algorithms

In agreement with our main assumption in Section 2.2, we assume that progression within the cell cycle, apoptosis and the initiation of differentiation programs are initially blocked by specific inhibitory molecules. This would allow for newly formed cells to remain in the first stage of the cell cycle (G1) before choosing a given cell fate. During this stage, membrane receptors interacting with external signals dictate the dynamics of inhibitors, thus controlling the eventual decision of the cell (see Figure 3). The effect of the complexes formed by membrane receptors and external cues in the inhibition (resp. activation) of any cell fate choice takes place through an increase (resp. decrease) in the amount of the inhibitory molecule controlling this

Signal	Source	OCL	OBL	OBA
R	OBA	Activation <i>Survival</i>	-	-
S	OCY	Apoptosis Inhibition	<i>No proliferation</i> No differentiation <i>Apoptosis</i>	No proliferation No differentiation Apoptosis
T	OCY OBL OBA	-	<i>Proliferation</i> Differentiation <i>Survival</i>	No proliferation

Table 2.2: **Generic signals to be considered in our model and a list of the actions they induce on cell types of a BMU**

choice. Cell fate is decided when the first of the inhibitors considered reaches its critical threshold.

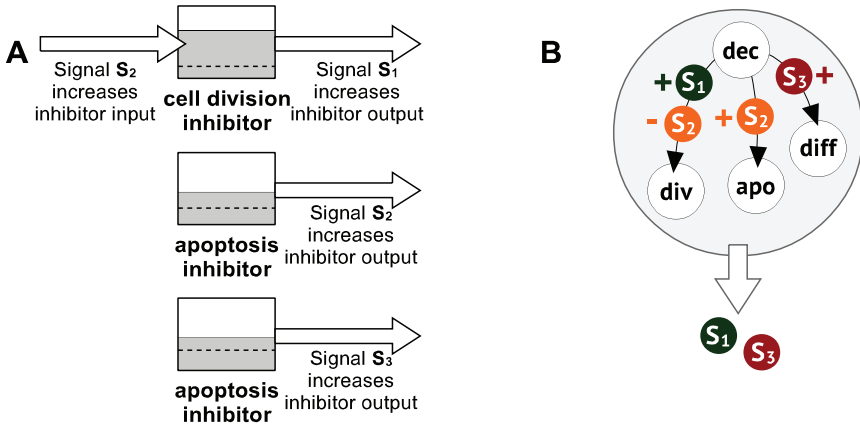


Figure 2.3: **Cell fate decision algorithm.** **A)** The first stage of the cell cycle is a decision phase (dec). During this phase, membrane receptors interact with specific external signals (S_1 , S_2 and S_3 in the picture). As a result, changes in the concentrations of inhibitory molecules blocking progression into the cell cycle (div), apoptosis (apo) and differentiation (diff) are induced. In the particular case considered, signal S_1 competes with S_2 to induce and inhibit cell division respectively. Signal S_2 induces the initiation of the apoptosis program, while signal S_3 leads to cell differentiation. Each inhibitor has a critical threshold (dashed line) that has to be reached to trigger the corresponding cell action. **B)** Diagram of the cell decision algorithm described in A). We remark that signals controlling cell fate do not need to be produced by the cell itself. In this case, for instance, the cell releases signals S_1 and S_3 , while signal S_2 is produced by other cell types.

The inhibitor dynamics will be assumed to be of the following form:

$$\begin{cases} c'(t) = f_c(R, S, T) \\ a'(t) = f_a(R, S, T) \\ d'(t) = f_d(R, S, T), \end{cases} \quad (2.1)$$

where $c(t)$, $a(t)$ and $d(t)$ respectively denote the concentrations of division, apoptosis and differentiation inhibitors at time t and f_c , f_a , and f_d are functions of three external signals S , R and T . For simplicity, we shall assume in the sequel such functions to be piecewise linear, and will next describe the main details of the decision algorithm for any cell type in a BMU.

Osteoblasts (OBL)

Osteoblasts (OBL) are initially located at the interface between bone matrix and bone marrow. In normal conditions, osteoblasts homeostasis is maintained by a continuous cell turnover, involving both division and apoptosis [41]. If a remodeling process starts, osteoblasts can also differentiate into active osteoblast (OBA). OBLs can therefore choose among three alternative programs. In this work we will not consider OBL division and apoptosis, which are therefore assumed to balance each other during the process, and will focus on OBL activation during bone remodeling. Activation is known to be mainly blocked by the release of sclerostin by osteocytes [5, 8]. This will be modeled by assuming that signal S , produced by osteocytes, increases the amount of a differentiation inhibitor in OBLs, denoted by d_B , according to the following dynamics:

$$\begin{cases} d'_B(x, y; t) = \alpha_B^{S_1} S(x, y; t) - \alpha_B^{S_2}, & \text{if } d_B < D_B \text{ and box at } (x, y) \text{ is adjacent to bone} \\ d'_B(x, y; t) = 0 & \text{otherwise,} \end{cases} \quad (2.2)$$

where (x, y) denotes the position of the OBL, D_B is the maximum amount of inhibitor that can accumulate within a OBL, $S(x, y; t)$ is the amount of signal S at location (x, y) at time t and α_B^1 and α_B^2 are positive parameters. During a bone remodeling process, osteoblasts remain in their original positions, delimiting the BRC [9]. Accordingly, OBLs do not move in our model.

Active osteoblasts (OBA)

Once differentiated, OBLs become active osteoblasts (OBA). OBAs have three possible choices: cell division, cell death and differentiation into osteocytes (OCY). We postulate that OBA division, apoptosis and differentiation are inhibited by molecules whose concentration are denoted by c_A , a_A and d_A . Furthermore, we assume that following activation OBAs can only divide, which leads to the layer of OBAs to progressively cover the surface of the cutting cone (see Section 2.3.2 below). We assume that during this process the existence of OBA that are not in contact with the bone surface blocks both the differentiation of OBAs into OCY and their apoptosis. This

can be achieved, for instance, by the interchange of molecules through gap junction communications between cells. When all OBAs are attached to the bone matrix, OBAs start to synthesize osteoid matrix, and can also differentiate into OCY or die, depending on the concentration of signal S in the environment. Differentiation into OCY will also be assumed to be blocked by cell contact with existing OCY, so that only OBAs whose distance to OCY is larger than a threshold can differentiate. These behaviors are modeled by means of the following equations:

$$\begin{cases} c'_A(x, y; t) = -\alpha_A^T T(x, y; t), & \text{if box at } (x, y) \text{ is not adjacent to bone} \\ c'_A(x, y; t) = 0 & \text{otherwise,} \end{cases} \quad (2.3)$$

where (x, y) denotes the position of the OBA, $T(x, y; t)$ is the amount of signal T at location (x, y) at time t and α_A^1 is a positive parameters.

When all OBAs are attached to the bone surface, cell division is no longer possible for lack of space, and osteoid production, apoptosis and differentiation into OCY can take place, according to these equations:

$$\begin{cases} a'_A(x, y; t) = -\alpha_A^{S_1} S(x, y; t) \\ d'_A(x, y; t) = \begin{cases} \alpha_A^{S_2} S(x, y; t) - \alpha_A^{S_3}, & \text{if distance to boxes occupied by OCY is less than } \delta_A \\ 0 & \text{otherwise} \end{cases} \end{cases} \quad (2.4)$$

where $S(x, y; t)$ is the amount of signal S at location (x, y) at time t and α_A^i (for $i = S_1, S_2, S_3$) are structural positive parameters and δ_A is a positive variable parameter. Parameter δ_A allows to model the effect of cell-to-cell contact inhibition by OCYs on OBAs activation, resulting from gap junction communications between cells [8].

Osteoclast precursors (OCP)

OBA can recruit OCP to the bone remodeling zone by secreting signal R , while signal S inhibits OCP recruitment. We will not consider in the model OCP division and apoptosis, and assume instead that enough OCP are available in the bone marrow (in particular, in the locations adjacent to those occupied by OBAs). OCPs attach to the bone surface upon their recruitment by OBAs, after which they become active osteoclasts (OCL). We assume that OCP activation is blocked by inhibitor d_P , whose dynamics is modeled as follows:

$$d'_P(x, y; t) = -\alpha_P^R R(x, y; t) + \alpha_P^S S(x, y; t) \quad (2.5)$$

where $R(x, y; t)$ and $S(x, y; t)$ are respectively the amounts of signal R and S at location (x, y) at time t and α_P^1 and α_P^2 are positive parameters.

Osteoclasts (OCL)

Once recruited to the BRC, OCPs become active osteoclasts (OCL) and start dissolving the bone matrix, thus leading to the formation of a cutting cone. OCLs are

assumed to be endowed with two alternative apoptosis pathways. One is controlled by signal R and ensures that OCLs die in the absence of activated OBA. A second pathway is controlled by signal S , produced by OCYs, and determines the depth that will be reached by the cutting cone (the progression of OCLs into old bone is described in Section 2.3.1). In particular, OCLs in locations with high concentrations of S will stop digging into the bone matrix and die. We will model the apoptosis pathway controlled by signal S by assuming that cell death is blocked by inhibitor a_C , whose dynamics is given by following equations:

$$\begin{cases} a'_C(x, y; t) = \alpha_C^{S_1} & \text{if } S(x, y; t) > \alpha_C^{S_2} \\ a'_C(x, y; t) = 0 & \text{otherwise,} \end{cases} \quad (2.6)$$

where $S(x, y; t)$ is the amount of signal S at location (x, y) at time t and α_C^1 and α_C^2 are positive parameters.

The algorithms just described for the cell types in a BMU are summarized in figure 4.

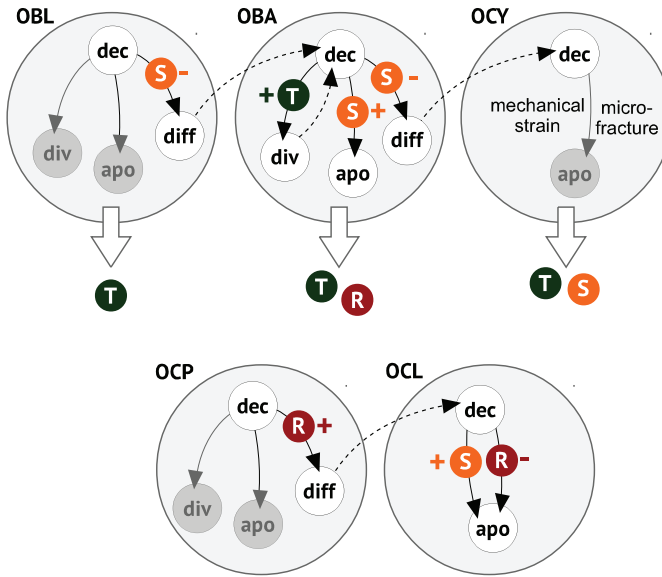


Figure 2.4: **A proposal for BMU software.** Signals R , S and T (in small circles) are produced by the cell types listed. They may inhibit (-) or induce activation (+) on the actions considered. Activation results from double inhibition, that is by lowering the concentration of an inhibitor. Within any cell type, possible decision choices are indicated by thin arrows. Dashed arrows correspond to a starting decision stage in a newly formed cell. Releasing of signals by any cell type (for instance, R and T in the case of active osteoblasts) is denoted by thick, white arrows.

2.3.2 Spatial dependence in the model

In order to account for the effect of signals on cell decisions within a BMU, the spatial disposition of both cells and molecules should be explicitly taken into account. To do that, we will consider a 2 dimensional cross-section of bone adjacent to a section of bone marrow by means of a cellular automaton (CA). More precisely, the bone section considered will be thought of as a lattice divided in boxes of equal size, where any such box can either remain empty or be occupied by only one individual cell. In addition, boxes can contain different amounts of chemical cues. The dynamics of signals in the CA is summarized as follows. At any given time, they are produced by the corresponding cell types at constant rates. Signals are also assumed to undergo Arrhenius-type decay (meaning that their decay rate is proportional to their concentration) and to diffuse through the medium. We assume that diffusion occurs faster than internal cell processes. In order to account for these two time scales simultaneously, we model diffusion by calculating, at each box and each iteration step of the model, a weighted average of the amount of signals in neighboring positions (see Figure 5.A). Cells need not remain confined to fixed boxes in the lattice. Active osteoblasts and osteoclasts can decide to move anytime during the simulation. Such decision is made upon comparing the amount of different signals in their adjacent boxes; details about the movement of each cell type will be provided below. As a starting point we consider a population of osteocytes (OCY), regularly distributed within the bone matrix, and a layer of osteoblasts lining the bone section (see Figure 5.B). Simulations of the model are started after apoptosis of a group of osteocytes has occurred (see Figure 5.C).

2.3.3 Cell movements

In this section we will describe the movements of active osteoblasts and osteoclasts during a bone remodeling event.

Active osteoclasts

After osteocyte apoptosis, osteoclasts are recruited into the BRC by active osteoblasts. Once activated, osteoclasts start to remove old bone, thus giving rise to the appearance of “cutting cones”, that may reach a variable depth into old bone matrix, depending on the number of apoptotic osteocytes [22, 23]. We will assume that osteoclasts remove bone at a rate that depends on the amount of signal S , thus simulating the inhibitory effect that has been described for signals produced by osteocytes of osteoclasts activity [23]. We will assume that osteoclasts move to and adjacent box once they have removed bone in their current position.

Bone resorption will be modeled by means of the following equations:

$$\begin{cases} b'_C(x, y; t) = -\alpha_C^{S_3} \left(1 - \frac{S(x, y; t)}{\alpha_C^{S_4}}\right) & \text{if } S(x, y; t) \leq \alpha_C^{S_4} \\ b'_C(x, y; t) = 0 & \text{otherwise,} \end{cases} \quad (2.7)$$

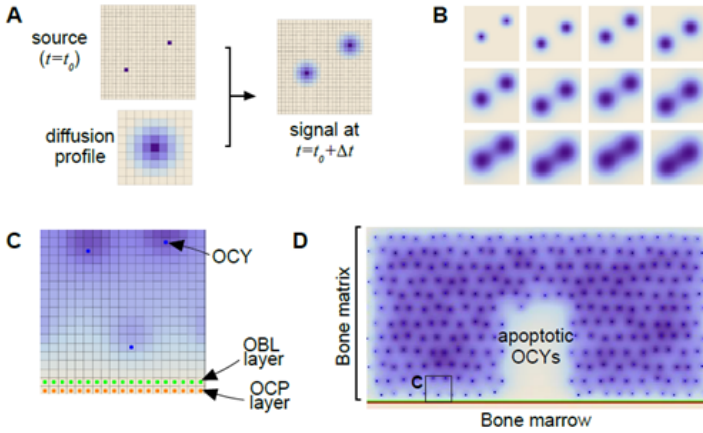


Figure 2.5: **Spatial aspects of the model.** **A)** Signal diffusion takes place at a different scale than cell decisions. Let Δt be the characteristic time step for cell processes. In order to model signals diffusion, we calculate the profile resulting from cells diffusing during this time interval. Diffusion can then be modeled at this characteristic time by applying the corresponding profile to any source of signals in the CA. **B)** Snapshots of a signal diffusion from the source shown in A. Time increases from left to right and from top to bottom. **C)** Spatial arrangement of the main elements of the model. Bone matrix is locally represented by means of a lattice consisting of equal-size boxes, each able to accommodate one cell. The lower boundary of the box considered in B is represented as lined with an osteoblast layer, lying upon a layer of osteoclast precursors. **D)** Initial configuration of the model. At a selected place within the bone matrix, osteocytes (blue dots) may undergo apoptosis, thus triggering BMU operation in the corresponding region (blank). Lattice element considered in B) is represented her for comparison purposes (see lower left corner). Shades of blue represent different concentrations of signals in each box.

where $S(x, y; t)$ is the amount of signal S at location (x, y) at time t and $\alpha_C^{S_3}$ and $\alpha_C^{S_4}$ are positive parameters.

Active osteoblasts

Active osteoblasts move from their original position in the interface between bone matrix and bone marrow to the inner surface of the cutting cone in order to secrete new osteoid matrix. Osteoid production is also accompanied by active osteoblasts movement, this time in the opposite direction. In our model, the movement of active osteoblasts will be modeled as a consequence of cell division in the first stages of the bone formation phase. The production of osteoid will, in turn, entail the apoptosis

and differentiation of some of the activated osteoblasts, which will result in the movement of the active osteoblast layer back to the position occupied by osteoblasts before the remodeling event (see Appendix A and figures A.1 and A.2 for details).

2.4 Results

In this Section we present some results obtained upon simulation of the model whose elements have been described in our previous Section. To keep the flow of the main arguments here, we postpone some technical details to Appendix A at the end of the paper. Specifically, the reader will find there a flow chart describing the order in which the corresponding algorithms are applied, as well as a list of the parameters used in the simulations whose results will be shown below. Concerning this last issue, we wish to emphasize that no parameter-fitting attempt has been made here. Our concern is to show that the model proposed has not only the potential to reproduce standard features in bone remodeling, but also to draw conclusions about the manner in which this process is carried out that could not be a priori anticipated before simulating that model. We will thus describe a choice of parameters for which such goals are achieved, although we do not claim that these values are actual ones. Parameters appearing in the actual BMU software should be of a structural nature, and their precise values have to be determined experimentally. In fact, the circuitry underlying BMU operation is expected to be rather sensitive to small variations in such parameter values, a fact repeatedly observed in processes selected during evolution. An example of such situation is provided by the Krebs cycle [42, 43] which consists in a network of biochemical reactions taking place exactly at very precise rates and proportions. We next succinctly describe some of the conclusions drawn from the simulation of the algorithms described in Appendix A.

2.4.1 The BMU software proposed successfully recapitulates bone remodeling

Upon induction of osteocyte apoptosis in a region, the cell algorithms proposed sequentially describe the manner in which bone remodeling occurs there. See Figure 6 below.

2.4.2 The size of the BRC adapts to the number of apoptotic OCY

The model proposed can be run when OCY apoptosis is assumed to occur in regions of different sizes. In each case, the area of the corresponding Bone remodeling Compartment (BRC) is shown to depend on the extent of the induced OCY apoptosis. See Figure 7.

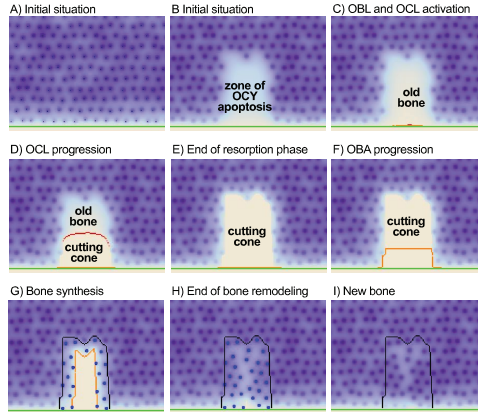


Figure 2.6: **Snapshots corresponding to sequential stages in a bone remodeling event.** **A**) A planar bone region is considered where active osteocytes (OCY, blue dots) are regularly distributed. Osteoblasts (OBL, in green) are located at the lower side, which represents the interface between bone and bone marrow. **B**) OCY apoptosis is induced in a subset (in white) of the previous region, which leads to a drop in OCY inhibitory action in that place. **C**) Lack of enough osteocyte inhibition results in OBL activation, and the recruitment of osteoclast precursors which differentiate into active osteoclasts, OCL (in red). **D**) OCL form cutting cones that move into the apoptotic region destroying old bone (bone resorption). **E**) OCL- driven resorption proceeds until the inhibitory effect of the remaining osteocytes precludes further OCL progression. **F**) Activated osteoblasts (OBA, in orange) move in the wake of OCL. **G**) OBA move inward from the OCL- lined cutting cone boundary secreting osteoid matrix. Part of them subsequently differentiate into OCY (blue dots). The limit of the cutting cone is shown in black. **H**) When remodeling is finished, a new distribution of osteocytes is achieved in the remodelled region, and **I**) new bone is eventually formed.

2.4.3 Osteoclast lifespan depends on the depth of the BRC

A prediction of the model is that average osteoclast lifespan is not a priori determined, but depends instead on the size of the region where bone remodeling has to be performed. This fact is illustrated in Figure 8 below, where mean OCL lifespan is plotted in terms of BRC depth.

2.4.4 The BMU software is robust to signal noise

As we have seen above, the operation of cells within a BMU depends on cell-to-cell communication by means of signals that diffuse through the bone matrix. The coupling of old bone resorption and new bone formation can therefore be affected by signal noise due, for instance, to bone matrix spatial heterogeneity. In figure 9 we

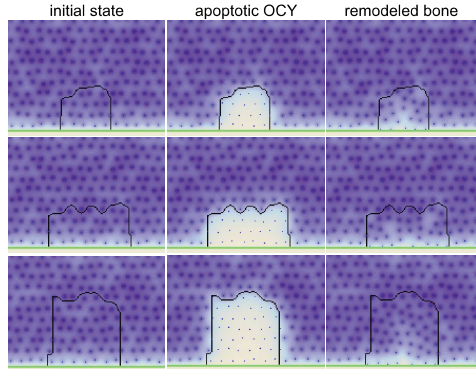


Figure 2.7: **Simulation of three different scenarios of OCY apoptosis.** Images correspond to results obtained in each case after the simulation of the model since OCY apoptosis until the end of the remodeling process. The edge of the resulting cutting cone is depicted in black. The shape and size of the resulting BRC is determined in each case by the region where OCY apoptosis has occurred.

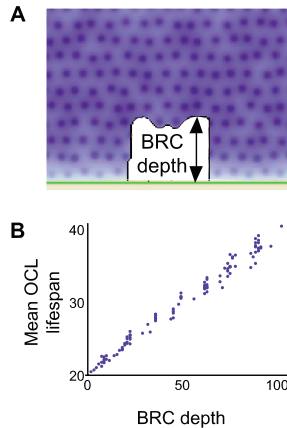


Figure 2.8: **Dependence of OCL lifespan on BRC size.** **Left)** A region where bone resorption has occurred following OCY apoptosis is depicted. BCR depth is defined there as the longest distance within that region measured perpendicular to its lower side. **Right)** A plot of average OCL lifespan during bone remodeling events in terms of BRC depth obtained after simulations of the model (each dot corresponds to a simulation). Note that OCL live longer when BRC is larger.

show that the suggested BMU software is robust to environmental noise.

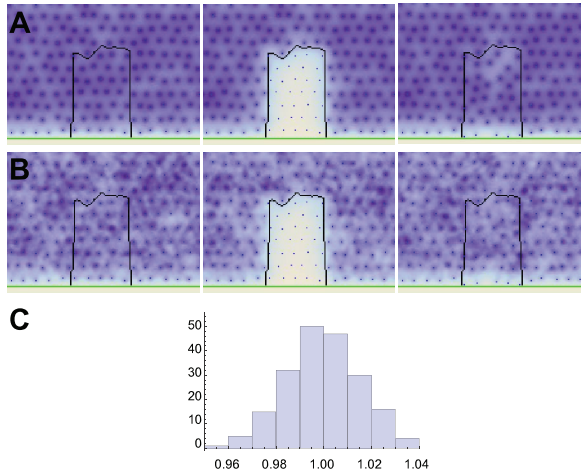


Figure 2.9: **Effect of signal noise in BMU operation.** **A)** Simulation corresponding to a bone remodeling without noise in signal S diffusion. The initial situation is depicted in the left figure. The shape of the cutting cone is marked in black. The region of apoptotic OCYs is shown in the center. The right picture corresponds to the new bone after remodeling. **B)** In spite of noise, both the resulting cutting cone and the new distribution of OCY is similar to A. **C)** Histogram of the rate between the number of newly formed OCY in the BRC after bone remodeling with and without noise (the result was obtained after 200 simulation of the model).

2.5 Discussion

In this work we have proposed and analyzed a minimal model for bone remodeling carried out by Bone Multicellular Units (BMUs) as part of their routine activity to replace old bone by new one, a process which is often triggered by changes in mechanical load. We have already recalled that such remodeling is continuously taking place during human life, so that on average the whole skeleton is renewed every 10 to 15 years [44]. BMUs activity is usually carried out at small regions, say about 4000 microns in width [45] and therefore the total number of cells involved in each remodeling event is comparatively small. The previous length scale can be also used to characterize micro-fractures (arising for instance from physical exercise) which are also self-repaired in the same manner. BMUs operation can thus be viewed as the basic building block to keep homeostasis in bone tissue. When normal function in bone is compromised by large-scale hazards (say, fractures), more sophisticated repair mechanisms, involving in particular inflammatory signals, blood clot formation and the production of different callus templates for bone repair are involved, which have not been discussed here.

Our goal in this work is to identify, by means of a mathematical model, a minimal algorithm for BMU operation. To do this, we have kept to a few basic principles.

First, at any time during that process, each cell within the different lineages present in a BMU should individually decide one among a restricted set of actions: divide, die or differentiate. Such choice is not assumed to be random, but determined by feedback from the surrounding medium into the internal dynamics of molecules which act as decision inhibitors. No previous planning is presupposed, genetically or otherwise. Second, only a minimal number of signals are selected that allow for BMU functioning. As recalled in Section 2, all elements retained have been shown to be actually in place in working BMUs. In particular, cell decision inhibitors have been identified, and effects induced by the signals proposed have been shown to be caused by chemical mediators experimentally detected. However, we have not aimed at producing a comprehensive model where all data currently known could be fitted. We have instead attempted to show what the basic ingredients of an operational BMU could be like. Implicit in this approach is the assumption that some signals already identified are multi-functional (thus yielding different effects in different cell lines) and that in general some signaling networks observed can be redundant, perhaps as a consequence of having been arrived at through different paths in the course of evolution. Notice, however that we do not claim that our proposal is the only possible one. In principle, there could be alternative minimal models for what we have called a BMU software. We believe however, that the degree of complexity retained in our model could not be significantly reduced by alternative mechanisms.

Selecting a minimal model has the advantage of dealing with a comparatively small number of parameters. Indeed, it is well known that a given phenomenon can be fitted by utterly different models, relying on different principles, upon appropriate choices of a suitable (and often rather modest) number of parameters appearing in them [46, 47]. We have shown herein that the parameters retained in our model can be selected so that BMU standard operation is reproduced and, importantly, consequences such as the dependence of osteoclasts lifespan on the size of the region to be repaired can be inferred that were not a priori clear before the model was simulated. We do not claim, however, that the results obtained provide a validation of the model. In our opinion, such validation could only stem from experimental determination of such values. This should be in principle possible, since most parameters retained are of a structural character (see pseudo-code guidelines in Appendix A). By that we mean that such values correspond to coefficients as for instance external signals/internal inhibitors interaction or maximal inhibitor accumulation within osteoblasts. Such performance rates might well have been evolutionary selected to remain confined within very narrow margins, as is the case with virtually all robust metabolic processes which have been unraveled so far [42, 43].

We conclude this discussion by briefly remarking on possible future directions arising from this work. To begin with, the experimental question of determining the operational parameters introduced in our model should be again stressed. If and when this is done, we would have in place a BMU chip structure to be used as a building block for operational purposes. On the other hand, one could simulate on models as that presented here the impact of external cues in the modulation of the repair process, either to slow it down or to accelerate it. Finally, as the

size of the region to be repaired increases, a threshold should be reached beyond which inflammatory signals become relevant, and a new and more complex stage is entered. Understanding the matching between these two cases could be instrumental in designing techniques to foster bone fracture repair. We intend to pursue some of these subjects elsewhere.

Bibliography

- [1] J. M. Graham, B. P. Ayati, S. A. Holstein and J. A. Martin (2013). The role of osteocytes in targeted bone remodeling: a mathematical model. *PLoS ONE* 8(5): e63884. doi:10.1371/journal.pone.0063884
- [2] M. L. K. Tate, J. R. Adamson, A. E. Tami and T. W. Bauer (2004). The osteocyte. *Int. J. Biochem. Cell Biol.* 36, 1: 1- 8.
- [3] F. F. Safadi, M. F. Barbe, S. M. Abdelmagid, M. C. Rico et al. (2009). *Bone structure, development and bone biology*. In Bone Pathology; 1.50. Humana Press.
- [4] R. L. Jilka, R. S. Weinstein, A. M. Parfitt and S. C. Manolagas (2007). Perspective : Quantifying osteoblast and osteocyte apoptosis: challenges and rewards. *Journal of Bone and Mineral Research* 22, 10: 1492-1501.
- [5] B. S. Noble, N. Peet, H.Y. Stevens, A. Brabbs et al. (2003). Mechanical loading: biphasic osteocyte survival and targeting of osteoclasts for bone destruction in rat cortical bone. *Am. J. Phys-Cell Phys.* 284, 4: C934-C943.
- [6] J. P. Bidwell, J. Yang and A. G. Robling (2008). Is HMGB1 an osteocyte alarmin ?. *J. Cell. Biochem.* 103, 6: 1671-1680.
- [7] A. M. Parfitt (2002). Targeted and nontargeted bone remodeling: relation to basic multicellular unit and progresi?n. *Bone* 30(1): 5-7.
- [8] E. F. Eriksen (2010). Cellular mechanisms of bone remodeling. *Reviews in endocrine and metabolic disorders* 11(4): 219-227.
- [9] E. M. Hauge, D. Qvesel, E. F. Eriksen, L. Mosekilde and F. Melsen (2001). Cancellous bone remodeling occurs in specialized compartments lined by cells expressing osteoblastic markers. *J. Bone. Min. Res.*16, 9: 1575- 1582.
- [10] I. H. Kalfas (2001). Principles of bone healing. *Neurosurgical Focus* 10, 4: 1-4.

- [11] T. A. Franz-Odenaal, B. K. Hall and P. E. Witten (2006). Buried alive: how osteoblasts become osteocytes. *Dev. Dyn.* 235, 1: 176-190.
- [12] N. A. Sims and T. J. Martin (2014). Coupling the activities of bone formation and resorption: a multitude of signals within the basic multicellular unit. *BoneKEY reports* 3.
- [13] S. V. Komarova, R. J. Smith, S. J. Dixon, S. M. Sims and L. M. Wahl (2003). Mathematical model predicts a critical role for osteoclast autocrine regulation in the control of bone remodeling. *Bone* 33: 206-215.
- [14] M. Ryser, S. Komarova and N. Nigam (2010). The cellular domains of bone remodeling: a mathematical model. *SIAM J. Appl. Math.* 70: 1899-1921.
- [15] J. M. Graham, B. P. Ayati, S. A. Holstein and J. A. Martin (2013). The role of osteocytes in targeted bone remodeling: a mathematical model. *PLoS ONE* 8(5), e63884.
- [16] A. G. Robling, A. B. Castillo and C. H. Turner (2006). Biomechanical and molecular regulation of bone remodeling. *Annu. Rev. Biomed. Eng.* 8: 455-498.
- [17] K. T. Steeve, P. Marc, T. Sandrine, H. Dominique and F. Yannick (2004). IL-6, RANKL, TNF- α /IL-1: interrelations in bone resorption pathophysiology. *Cytokine & growth factor reviews* 15 (1): 49-60.
- [18] B. S. Noble (2008). The osteocyte lineage. *Archives of Biochemistry and Biophysics* 473, 2: 106-111.
- [19] G. Chen, C. Deng and Y. P. Li (2012). TGF- β and BMP signalling in osteoblast differentiation and bone formation. *Int. Journal of Biological Sciences* 8, 2: 272.
- [20] R. Marsell and T. A. Einhorn (2011). The biology of fracture healing. *Injury* 42, 6: 551-555.
- [21] X. Cao (2011). Targeting osteoclast- osteoblast communication. *Nature Medicine* 17,11: 1344.
- [22] T. J. Heino, T. A. Hentunen and H. K. Väänänen (2002). Osteocytes inhibit osteoclastic bone resorption through transforming growth factor- β ? Enhancement by estrogen. *J. Cell. Biochemistry* 85, 1: 185-197.
- [23] G. S. Stein, J. B. Lian and T. A. Owen (1990). Relationship of cell growth to the regulation of tissue-specific gene expression during osteoblast differentiation. *The FASEB Journal* 4, 13: 3111-3123.
- [24] J. M. Hock, V. Krishnan, J. E. Onyia, J. P. Bidwell, J. Milas and D. Stanislaus (2001). Osteoblast apoptosis and bone turnover. *Journal of Bone and Mineral Research* 16, 6: 975-984.

- [25] W. J. Boyle, W. S. Simonet and D. L. Lacey (2003). Osteoclast differentiation and activation. *Nature* 423 (6937): 337-342.
- [26] S. L. Teitelbaum (2000). Bone resorption by osteoclasts. *Science* 289 (5854): 1504-1508.
- [27] B. S. Noble and J. Reeve (2000). Osteocyte function, osteocyte death and bone fracture resistance. *Molecular and Cellular Endocrinology* 159, 1: 7-13.
- [28] C. A. Mullen, M. G. Haugh, M. B. Schaffer, R. J. Majeska and L. M. McNamara (2013). Osteocyte differentiation is regulated by extracellular matrix stiffness and intercellular separation. *J. Mech, Behav. Biomed. Mat.* 28: 183-194.
- [29] E. Abe (2006). Function of BMPs and BMP antagonists in adult bone. *Ann. New York Acad. Sci.* 1068, 1: 41 - 53.
- [30] M. J. Christopher and D. C. Link (2008). Granulocyte Colony-Stimulating Factor induces osteoblast apoptosis and inhibits osteoblast differentiation. *Journal of Bone and Mineral Research* 23, 11: 1765-1774.
- [31] L. D. You, S. Weinbaum, S. C. Cowin and M. B. Schaffer (2004). Ultrastructure of the osteocyte process and its pericellular matrix. *The Anatomical Record A.* 278, 2: 505-513.
- [32] J. P. Reyes, S. M. Sims and S. J. Dixon (2011). P2 receptor expression, signalling and function in osteoclasts. *Front. Biosci. (Schol. Ed)* 3: 1101-1118.
- [33] M. Karin and T. Hunter (1995). Transcriptional control by protein phosphorylation: signal transmission from the cell surface to the nucleus. *Curr Biol* 5:747757.
- [34] R. L. Jilka, R. S. Weinstein, T. Bellido, A. M. Parfitt and S. C. Manolagas (1998). Osteoblast programmed cell death (apoptosis): modulation by growth factors and cytokines. *Journal of Bone and Mineral Research*, 13(5), 793-802.
- [35] C. F. Arias, M. A. Herrero, F. J. Acosta and C. Fernández -Arias (2014). A mathematical model for a T cell fate decision algorithm during immune response. *Journal of Theoretical Biology* 349: 109-120.
- [36] P. Ducy (2000). Cbfa-1: a molecular switch in osteoblast biology. *Dev. Dyn.* 219,4 ; 461-471.
- [37] P. Bialek, B. Kern, X. Yang, M. Schrock et al. (2004). A twist code determines the onset of osteoblast differentiation. *Dev. Cell* 6, 3 ; 423-435.
- [38] M. Zhao, M. Qiao, B. Oyajobi, G. R. Mundy and D. Chen (2003). E3 ubiquitin ligase Smurf 1 mediates core-binding factor β /Runx2 degradation and plays a specific role in osteoblast differentiation. *J. Biol. Chem.* 278, 30: 27939-27944.

- [39] W. Huang, S. Yang, J. Shao and Y.P. Li (2007). Signaling and transcriptional regulation in osteoblast commitment and differentiation. *Frontiers in Bioscience*: 12 ,
- [40] H. M. Ryoo, M. H. Lee and Y. J. Kim (2006). Critical molecular switches involved in BMP-2 induced osteogenic differentiation of mesenchymal cells. *Gene* 366, 1: 51-57.
- [41] J.F. Chau, W. F. Leong and B. Li (2009). Signaling pathways governing osteoblast proliferation, differentiation and function. *Histology and histopathology*, 24(12): 1593-1606.
- [42] D. L. Nelson, A. L. Lehninger and M. M. Cox. *Lehninger principles of biochemistry*. Macmillan, 2008.
- [43] O. Ebenhöh and R. Heinrich (2001). Evolutionary optimization of metabolic pathways. Theoretical reconstruction of the stoichiometry of ATP and NADH producing systems. *Bulletin of mathematical biology*, 63(1): 21-55.
- [44] M. Zaidi (2007). Skeletal remodeling in health and disease. *Nat. Med.* 13: 791-801.
- [45] A. M. Parfitt (2002). Targeted and non targeted bone remodeling: relationship to basic multicellular unit origination and progression. *Bone* 30, 1: 5-7.
- [46] H. C. Hemker, S. Kerdelo and R. M. W. Kremers (2012). Is there value in kinetic modeling of thrombin generation? *J. Thromb. Haemost.* 10: 1470-1477.
- [47] L. R. Ginzburg and C. X. J. Jensen (2004) . Rules of thumb for judging ecological theories. *Trends in Ecology and Evolution* 19, 3 ; 121-126.

Early stages of Bone fracture healing

3.1 Introduction

Bone repair is a robust physiological process which is constantly acting in healthy individuals. In particular, bone microfractures induced by exercise (including walking) are routinely self-healed without even being noticed, although large microfracture condensation may result in severe injury [39], [6]. Interestingly, bone self-repair makes use of key ingredients of the developmental program responsible for ossification during the embryonic stage [19], [18]. The sequence of events occurring after a bone fracture involves three phases: inflammatory, reparative and remodelling, each characterized by specific cellular, histological and biochemical features. The inflammatory phase has received relatively lower attention than the other two, in spite of its fundamental role in the subsequent evolution of the process.

In this chapter we propose and discuss a simple model to analyze the early stages of bone fracture repair. When a bone fractures, several blood vessels break and a mass of clotted blood is formed at the injury site. This fracture hematoma has a little effect to stabilize the bone, but it provides a first bridge between the two bone fragments and thus keeps both pieces lined up for mending. A key ingredient in this stage is the formation of the first elastic, fibrin-collagen scaffold (the so-called early fibrous callus, **EFC**) which provides a first consistent scaffold for mesenchymal cells to settle and differentiate to fibroblasts, chondrocytes and osteoblasts, to eventually form a bony bridge between the two fragments. The corresponding process, which is an essential starting point for subsequent bone healing, takes place in a comparatively short period: no more than 48 hours in the case of thin induced fractures in mice [21]. More precisely, we shall pursue the following goals: (i) to estimate the characteristic times of the main events leading to **EFC** formation, and (ii) to ascertain their dependence on the kinetics of key underlying mechanisms as platelet activation, fibrin polymerization and fibrin clot remodelling mediated by fibroblasts. We will not be directly concerned here with mechanical effects, which become particularly relevant

at later stages, as **EFC** becomes a cartilaginous callus (**CC**) on which different types of bone tissues are formed upon remodelling of **CC** through a sequence of processes which result in changes in the composition and mechanical properties of previous scaffolds [21], [20].

Our plan is as follows. In Section 2 below we review basic known biological facts concerning the main events in fracture repair, particularly during the early stage to be considered. We then discuss in Section 3 a mathematical model whose analysis will allow us to estimate several characteristic times of the process under consideration. The first of them corresponds to the formation of a fibrin blood clot, the earliest structure generated during the process of bone repair. The onset of such a clot, which in spite of its poor mechanical properties provides a first bridge to join both sides of the fracture and is therefore crucial for bone repair [50] is characterized here as a phase transition in a polymerization event. Its timing is estimated in terms of the various physiological processes (thrombin-induced activation, fibrin polymerization,...) involved.

Once this fibrin network is in place, attention is paid to a first, and crucial, remodelling effect. This results from the release of collagen over the fibrin net, which is deposited by fibroblasts arising from asymmetric division of mesenchymal stem cells (**MSCs**) recruited from neighbouring regions (periosteum). The timing of this event is kept track of by means of the motion of a front of **MSCs** proceeding inwards from the borders of the fracture gap. Such motion is chemotactically induced by growth factors released by activated platelets trapped within the fibrin clot [54], [24]. As it turns out, substantial insight about the process considered is derived from the study of a particular asymptotic limit, namely the case where fibrin clotting is triggered by an instantaneous thrombin discharge. Under such assumption, our model can be explicitly solved, which permits a detailed discussion of the influence of the different biological processes involved. Estimates for the characteristic times obtained in Section 3 are then provided in Section 4. Finally, a discussion on the results obtained as well on possible future directions is gathered in a concluding Section 5.

We point out that mathematical models of different aspects of ossification and bone repair have received considerable attention in recent years [35],[2],[23],[16],[44]; for later repair stages see also [41], [40], [45]. Some issues similar to those addressed in this work have been also discussed in related biological problems as wound healing, which shares a number of features with bone repair [38], [42], [32] in particular during the early stages here considered.

3.2 Basic facts on bone fracture healing. The first 48 hours

When bone fracture occurs, damage is induced on a variety of tissues including surrounding muscular cells and periosteum as well as on bone itself. Bone is a highly vascularized tissue, and its fracture leads to many blood vessels across the

fracture line being broken . Blood then runs away from disrupted vessels to the medullary canal between the fracture ends and rapidly coagulates to form a clot. On the other hand, immediately after fracture the resulting necrotic material induces an intense inflammatory response including widespread vasodilation, plasma exudation, edema and recruitment of acute inflammatory cells [9]. As a consequence, a complex hematoma is generated that is of major importance for the beginning of bone healing, since it provides a first bridge between separated fragments of bone [50]. Such hematoma plays a very small mechanical role in immobilizing the fracture, but it serves as a fibrin scaffold and provides an adequate microenvironment over which repair cells may settle to perform their function.

Formation of hematoma is a comparatively fast process. In the case of thin induced fractures in rat tibia, a case which will be considered here for comparison purposes, the fracture gap is about 2.5 mm in average, and hematoma can be observed by optical microscopy at about 3 hours after fracture induction. See Figure 1 below.

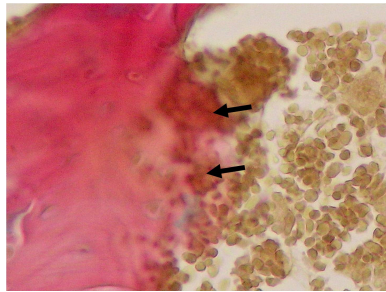


Figure 3.1: Blood clot between the ends of a bone fracture. Bone tissue is stained in pink whereas blood tissue has a brownish color. The immediate ends of the fracture border contain necrotic material (arrows). Picture take from tibia from a 35 days old rat, 6 hours after fracture.

A key constituent of hematoma is a fibrin net. Immediately after bone breaking, a coagulation process starts. Thrombin generated by blood vessel disruption induces the cleavage of fibrinogen present in blood to yield fibrin monomers, which quickly polymerize afterwards. In this manner a fibrin net is generated that in 6 to 8 hours connects both sides of the fracture and provides a first scaffold on which bone will eventually be produced [21], [15]. Importantly, when fracture occurs, a number of growth factors (**BMP**, **VEGF**, **PDGF**, ..) are released within the fracture gap [5]. Such substances will mediate subsequent steps in fracture repair.

As soon as a fibrin clot begins to form, new functional blood vessels as well as specific cell populations are recruited from the fracture boundaries. The cells involved directly in the repair of fractures are of mesenchymal origin and of a pluripotential nature. For definiteness we shall refer to such precursors as mesenchymal stem cells (**MSCs**) in the sequel. **MSCs** move in the wake of the new vascular bed created by incoming blood vessels. The latter can be seen within 6 to 12 hours near the fracture boundaries and between 24 to 48 hours they have invaded the whole fracture gap

[51]. See Figure 2 below where images taken 24 hours after fracture induction are presented.

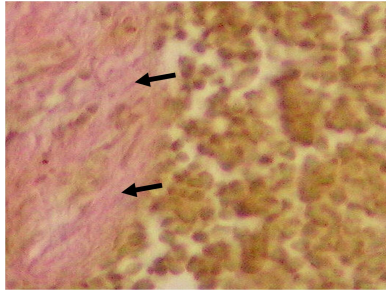


Figure 3.2: Early remodeling can be perceived in hematoma 24 hours after fracture, with fibrillar material being found in some regions of the blood clot represented in pink (arrows). Bone depicted in brown.



Figure 3.3: Image showing early invading cells derived from the cambium layer of the periosteum at the border of the fracture 24 hours after fracture. Such cells show morphology of mesenchymal cells (arrows).

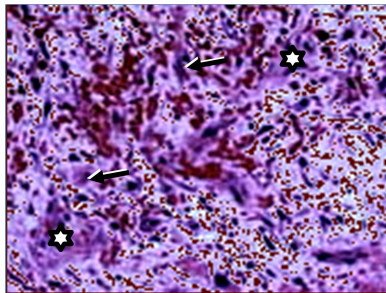


Figure 3.4: Picture representing a EFC being formed 24 hours after fracture. An increasing number of invading cells is observed (arrows) and partial reabsorption of the hematoma can be noticed (stars)

MSCs are chemotactically recruited from the fracture borders by chemical cues released from activated platelets trapped in the fibrin clot [30] (see Figure 3.3). **MSCs** may sustain either symmetric or asymmetric division [36]. Symmetric division, whereby a **MSC** gives raise to two new **MSCs**, takes place whenever their initial number is not enough to keep the healing process in time. On the other hand, when a **MSC** reaches the fibrin net, it can undergo asymmetric division, thus giving raise to one **MSC** and one differentiated cell, which may be of various types: fibroblasts, chondrocytes or osteoblasts depending on microenvironment stimuli and on the stresses they are subject to [36] [61], [31]. In particular, such lineages are known to depend on the density of the net on which division takes place [11], [14], [48]. Cell replication is stimulated by some of the growth factors present, whose action is in turn dependent on the unfolding of the fibrin clot. In particular, anchorage into the net significantly extends the half-life of growth factors with respect to that of freely diffusing ones [49], [60].

Specifically, the first type of asymmetric division takes place over a low-density fibrin clot and gives raise to fibroblasts. Once attached to the net, fibroblasts secrete a number of substances (collagens) which stick to the clot and change its mechanical properties [14], [48]. The resulting network, called early fibrous callus (**EFC**) is in place between 24 to 48 hours after bone break up (see Figure 3.4). It has larger mechanical stability than its preceding fibrin net, although not enough to ensure working stability to the healing bone. Such stability will be achieved through subsequent remodeling processes. In particular, upon sticking to a collagen-enriched fibrin net, **MSC** can again undergo asymmetric division that now gives raise to one **MSC** and one chondrocyte [36], [11]. This new type of cell interacts with the existing net and produces a more stable compound, called cartilaginous callus. Bone formation properly begins in a subsequent remodeling phase. At that stage, cartilaginous callus is replaced first by trabecular and then by lamellar bone [55] through a process similar to endochondral ossification. These later stages will not be considered in this work.

3.3 A mathematical model for the formation of a fibrin-collagen callus template.

In this Section we formulate and analyze a mathematical model to describe the early stages of cartilaginous callus formation in a fracture. For simplicity we specialize here to a one-dimensional case, and assume that the fracture gap is located at an interval centered around the origin, say $\Omega = \left(-\frac{L}{2}, \frac{L}{2}\right)$, with $L > 0$. Our model is of a modular character, and contains a series of basic units which are activated in sequential order. These will be described below.

3.3.1 Generation of fibrin monomers upon thrombin-induced fibrinogen cleavage.

Right after a fracture is generated, a number of substances arising from broken blood vessels are allowed to enter in contact with leaked blood. The actual sequence of biochemical events thus triggered is known to involve several agents [17], [43]. However, a common simplifying assumption consists in considering that complex process as driven by the action of the enzyme thrombin (obtained from its inactive precursor prothrombin) which cuts inactive fibrinogen molecules present in blood, thus giving raise to fibrin monomers. The latter then quickly polymerize to produce a fibrin clot. It is customary to describe thrombin generation by means of curves of the form represented in Figure 3.5, below ([17], [8]).

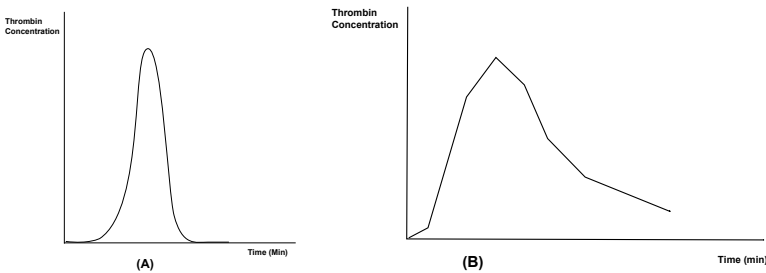


Figure 3.5: Typical thrombin profiles (adapted from [17], [8]). (A) About 95% of thrombin is generated as a consequence of positive feedback processes involving coagulation factors **FVIII**, **FIX** and **FX** [17], [37]. (B) dependence of thrombin concentration on time in some experimental settings, when anticoagulant factors are kept below haemostatic levels [8].

As mentioned in the caption of Figure 3.5, the sequence of events leading to thrombin generation include a number of feedback loops of an activator-inhibitor nature involving several coagulation/anticoagulation factors ([17], [25], [27]). Given that large uncertainties remain about the order and rates of the corresponding chemical reactions ([12], [57]), we have resorted here to a simplified modelling approach, which is now described. Let us respectively denote by $F(t)$, $\theta(t)$ the concentration of fibrinogen and thrombin (assumed homogeneous in space) at time t . We postulate that fibrinogen is removed by thrombin according to a second order kinetics

$$\dot{F} = -k_g F\theta \quad \text{for some } k_g > 0, t > 0 \quad (3.1)$$

whereas at $t = 0$, when fracture occurs, one has that

$$F(0) = F_M > 0 \quad (3.2)$$

for some physiological concentration F_M . We now consider an asymptotic limit of the profile sketched in Figure 3.5 A, namely the case of an instantaneous thrombin discharge at $t = T_M > 0$, that is:

$$\theta(t) = C\delta(t - T_M) \quad \text{for some } C > 0 \quad (3.3)$$

where $\delta(t - T_M)$ denotes Dirac's delta at $t = T_M$. Note that (3.1) and (3.3) represent a very fast chemical reaction for which the precise mathematical meaning of the governing differential equation has to be specified. In particular (3.1) is to be understood here as stating:

$$\frac{d}{dt}(\log F) = -k_g\theta$$

On integrating this equation and using (3.2) it follows at once that:

$$F(t) = \begin{cases} F_M & \text{for } t < T_M \\ F_M e^{-k_g C} & \text{for } t > T_M \end{cases} \quad (3.4)$$

Fibrinogen molecules cleaved by thrombin give rise to fibrin monomers, which subsequently polymerize to form large fibrin aggregates. Using classical polymerization theory ([53], [28], [25]) the corresponding process can be modelled by an infinite system of coagulation-fragmentation equations for the concentrations $F_k(t)$ of fibrin k -mers $k \geq 1$

$$\dot{F}_1 = k_g F \theta - F_1 \sum_{i=1}^{\infty} a_{1i} F_i + \sum_{i=1}^{\infty} b_{1i} F_{i+1} - k_r F_1 \quad (3.5)$$

$$\begin{aligned} \dot{F}_k = & \frac{1}{2} \sum_{m=1}^{k-1} a_{m,k-m} F_m F_{k-m} - F_k \sum_{i=1}^{\infty} a_{ki} F_i + \sum_{i=1}^{\infty} b_{ki} F_{i+1} \\ & - \frac{1}{2} \sum_{i+j=k} b_{ij} F_k - k_r F_k; \quad k = 2, 3, \dots \end{aligned} \quad (3.6)$$

where a_{kj} , (respectively b_{kj}) denote the coagulation rates between k -mers and j -mers (respectively the fragmentation rate at which k -mers are produced from the break-up of j -mers, $j > k$). Rates k_r correspond to polymer deactivation, and will be assumed to be independent of polymer length by simplicity. Assuming polymerization to occur according to classical Flory-Stockmayer theory, so that no polymer rings can be formed and coagulation rates are proportional to the number of the free available sites in each polymer, it turns out that

$$a_{ij} = k_p ((f - 2)i + 2) ((f - 2)j + 2)$$

([25], [28]) where f denotes the number of active functional sites in a fibrin monomer. Taking $f = 4$ ([59]) we eventually obtain

$$a_{ij} = 4k_p (i + 1)(j + 1) \quad (3.7)$$

On the other hand, assuming (i) the probability of a molecule of length k being cut by a fragmentation mechanism to be proportional to the number $(k - 1)$ of bonds and (ii) the probability to form a molecule of length i out of fragmentation of a molecule of length k ($k > i$) to be inversely proportional to the number of bonds, we obtain ([25]) that:

$$b_{ij} = 2k_b \quad \text{for some } k_b > 0 \quad (3.8)$$

A general discussion of the resulting system (3.5)-(3.8) is highly involved and will not be pursued here. However, considerable insight into blood-clotting dynamics is gained by making use of suitable auxiliary assumptions and simplifying hypotheses. To this end, for any integer $n \geq 0$ we define the n -moment M_n of the polymer distribution:

$$M_n(t) = \sum_{k=1}^{\infty} k^n F_k(t) \quad (3.9)$$

Note that $M_1(t)$ represents the total mass of the polymer distribution once the monomer mass has been normalized to one. Of particular interest here is the fact that the ratio (M_2/M_1) corresponds to the average molecular size. In classical Flory-Stockmayer theory a finite-time blow-up of that ratio marks the onset of a sol-gel phase transition, whereby a gel phase appears ([53]). Bearing this fact in mind, we say that a fibrin clot is formed as soon as that ratio develops a singularity at some time ([28], [25]). Upon replacing k_b by $3k_b$, it follows from (3.5)-(3.8) that the moments M_1 , M_2 satisfy:

$$\begin{aligned} \dot{M}_1 &= k_g F \theta - k_r M_1 \\ \dot{M}_2 &= k_g F \theta + 4k_p (M_2 + M_1)^2 - k_b (M_3 - M_1) - k_r M_2 \end{aligned} \quad (3.10)$$

Note that such a system is not in a closed form, since the third moment M_3 appears in equation for M_2 . To obtain a well posed problem we now set:

$$M_3 = \frac{M_2^2}{M_1} \quad (3.11)$$

As observed in [25] where this closure argument was proposed, (3.10) holds true in two extreme cases, namely when either only monomers exist or when all fractions are concentrated in a single, large cluster and no smaller fractions are present. However, one always has that $M_2^2 \leq M_1 M_3$ by Holder's inequality. Thus, when substituting (3.11) into (3.10), equality sign in the second equation for (3.10) has to be replaced by \leq there. Therefore, the closed system

$$\dot{M}_1 = k_g F \theta - k_r M_1 \quad (3.12)$$

$$\dot{M}_2 = k_g F \theta + 4k_p (M_2 + M_1)^2 - k_b \left(\frac{M_2^2}{M_1} - M_1 \right) - k_r M_2 \quad (3.13)$$

is satisfied by solutions M_1 to (3.12) and by subsolutions M_2 to (3.13).

3.3.2 Estimating fibrin clot formation

As it turns out, equations (3.12), and (3.13) can be explicitly solved under our current assumption (3.3). Notice that using (3.1), (3.12) can be rewritten in the form

$$\frac{d}{dt} (e^{k_r t} M_1) = k_g e^{k_r t} F \theta = -e^{k_r t} \dot{F}$$

it then follows that

$$M_1(t) = 0 \quad \text{for } t < T_M; \quad M_1(T_M) = F_M (1 - e^{-k_g C}) \equiv A \quad (3.14)$$

$$M_1(t) = A e^{-k_r(t-T_M)} \quad \text{for } t > T_M \quad (3.15)$$

Concerning the second moment, one also has that

$$M_2(t) = 0 \quad \text{for } t < T_M; \quad M_2(T_M) = A \quad (3.16)$$

Notice that the values $M_1(T_M) = M_2(T_M) = A$ are obtained from the fact that by (3.1), (3.2) and (3.13) the jump of M_1, M_2 at $t = T_M$ is provided by instantaneous activation of fibrinogen by thrombin at that time. We next point out that, on multiplying both sides in (3.13) by $e^{-k_r(t-T_M)}$ and upon noticing that $e^{-k_r(t-T_M)} = \frac{M_1(t)}{A}$ for $t > T_M$ (cf. (3.15)) one readily sees that $U(t) = \frac{M_2(t)}{M_1(t)}$ satisfies:

$$\frac{dU}{dt} = 4k_p A e^{-k_r(t-T_M)} (U + 1)^2 - k_b (U^2 - 1) \quad \text{for } t > T_M \quad (3.17)$$

$$U(T_M) = 1. \quad (3.18)$$

Equation (3.17) is of Riccati type. Since $U(t) = -1$ is a particular solution, its general solution can be sought in the form

$$U(t) = Y(t) - 1 \quad (3.19)$$

To better understand the consequences of the various kinetic processes retained in (3.17), the following situations will be separately considered:

1. **Case:** $k_p > 0, k_b = k_r = 0$. When fragmentation and deactivation are considered negligible with respect to coagulation, we obtain from (3.17) and (3.19) that

$$U(t) = \frac{1 + 8Ak_p(t - T_M)}{1 - 8Ak_p(t - T_M)} \quad (3.20)$$

which blows up at a time T_f given by

$$T_f = T_M + \frac{1}{8Ak_p} \quad (3.21)$$

2. **Case:** $k_p > 0$, $k_b > 0$, $k_r = 0$.

We now obtain from (3.17) and (3.19) that

$$U(t) = \frac{k_b + 4Ak_p(1 - e^{-2k_b(t-T_M)})}{k_b - 4Ak_p(1 - e^{-2k_b(t-T_M)})} \quad (3.22)$$

$U(t)$ blows up at $t = T_f$ if

$$1 - e^{-2k_b(T_f - T_M)} = \frac{k_b}{4Ak_p} \quad (3.23)$$

which requires

$$k_b < 4Ak_p \quad (3.24)$$

Therefore, large fragmentation rates preclude the formation of fibrin clots. When (3.23) holds, it follows from (3.23) that

$$T_f = T_M - \frac{1}{2k_b} \log \left(1 - \frac{k_b}{4Ak_p} \right) \quad (3.25)$$

Note that (3.25) reduces to (3.21) in the limit $k_b \rightarrow 0$. Moreover $T_f(k_b)$ is increasing in k_b , so that (3.21) provides a lower bound for (3.25) when $0 < k_b \ll 1$.

3. **Case:** $k_p > 0$, $k_b > 0$, $k_r > 0$.

When all kinetic rates are different from zero substitution of (3.19) into (3.17) leads to

$$\frac{dY}{dt} = f(t)Y^2 + 2k_bY; \quad f(t) = 4k_pAe^{-k_r(t-T_M)} - k_b \quad (3.26)$$

so that $Z = -\frac{1}{Y}$ solves

$$\frac{dZ}{dt} + 2k_bZ = f(t), \quad Z(T_M) = -\frac{1}{2}$$

whence

$$\begin{aligned} Z(t) &= e^{-2k_b(t-T_M)} \left(-\frac{1}{2} + \int_{T_M}^t e^{2k_b(s-T_M)} f(s) ds \right) \\ &= \frac{4Ak_p}{2k_b - k_r} \left(e^{-k_r(t-T_M)} - e^{-2k_b(t-T_M)} \right) - \frac{1}{2} \end{aligned} \quad (3.27)$$

for $t > T_M$ when $2k_b \neq k_r$, and:

$$Z(t) = 4Ak_p(t - T_M)e^{-2k_b(t-T_M)} - \frac{1}{2} \quad (3.28)$$

for $t > T_M$ and $2k_b = k_r$. Assume now that $2k_b > k_r$, then, on setting:

$$Q = \frac{4Ak_p}{2k_b - k_r} = \frac{4F_M(1 - e^{-k_g C})k_p}{2k_b - k_r} \quad (3.29)$$

it follows that $U(t) = \frac{M_2(t)}{M_1(t)}$ is given by:

$$U(t) = \frac{1 + Q \left(e^{-k_r(t-T_M)} - e^{-2k_b(t-T_M)} \right)}{1 - 2Q \left(e^{-k_r(t-T_M)} - e^{-2k_b(t-T_M)} \right)} \quad (3.30)$$

Let $g(t) = e^{-k_r(t-T_M)} - e^{-2k_b(t-T_M)}$ for $t \geq T_M$. Clearly $g(T_M) = 0$, $g(t) > 0$ for $t > T_M$ and $g(t)$ achieves a maximum at some time $t = t^*$. A straightforward computation yields that:

$$t^* = T_M + \frac{1}{2k_b - k_r} \log \left(\frac{2k_b}{k_r} \right) \quad (3.31)$$

$$m^* = g(t^*) = \left(\frac{2k_b}{k_r} \right)^{-\frac{k_r}{2k_b - k_r}} - \left(\frac{2k_b}{k_r} \right)^{-\frac{2k_b}{2k_b - k_r}} \quad (3.32)$$

Thus for $U(t)$ in (3.30) to blow up at time T_f , we need

$$2Qm^* \geq 1 \quad (3.33)$$

where Q , m^* are respectively given in (3.29) and (3.32). If (3.33) holds, one has that

$$T_f \leq T_M + \frac{1}{2k_b - k_r} \log \left(\frac{2k_b}{k_r} \right) \quad (3.34)$$

the case where $2k_b < k_r$ is similarly dealt with. Finally, when $2k_b = k_r$ blow up for $U(t)$ occurs if there exists $T_f > T_M$ such that

$$8Ak_p(T_f - T_M)e^{-2k_p(T_f - T_M)} = 1 \quad (3.35)$$

It is readily seen that (3.35) holds if $m^* = \max_{t > T_M} \left((t - T_M)e^{-2k_b(t - T_M)} \right)$ is such that $8Ak_p m^* \geq 1$. Since $m^* = (2ek_b)^{-1}$ in this case, the resulting condition reads:

$$4Ak_p > ek_b \quad (3.36)$$

We conclude this section by observing that our discussion can be extended to the case where (3.3) is replaced by

$$\theta(t) = C(x)\delta(t - T_M)$$

for some function $C(x)$. One just has to replace C by $C(x)$ in the corresponding estimates, as for instance in (3.21). Note that this implies that $T_f = T_f(x)$ so that different clot nucleation centers may be generated at different times.

3.3.3 Platelet activation and growth factor release

Besides cleaving fibrinogen, thrombin also mediates platelet activation [17]. Activation leads to platelets changing shape, sticking to each other and releasing the content of their storage granules [7]. In the sequel we will denote by $p_a(t)$ the concentration of activated platelets at time $t > 0$. Ignoring deactivation effects, we propose the dynamics of $p_a(t)$ to be given by:

$$\dot{p}_a(t) = \alpha(P_0 - p_a(t))\theta \quad \text{for } t > 0 \quad (3.37)$$

$$p_a(0) = 0 \quad (3.38)$$

Here θ stands for thrombin concentration, P_0 denotes the concentration of platelets at $t = 0$ and $\alpha > 0$ is an activation rate. Arguing as for (3.4) under assumption (3.3), equations (3.37), (3.38) yield at once:

$$p_a(t) = \begin{cases} 0 & \text{if } t < T_M \\ P_0(1 - e^{-\alpha C}) & \text{if } t > T_M \end{cases} \quad (3.39)$$

Upon activation, platelets are known to release a number of growth factors with mitotic and chemotactic effects, including members of the **VEGF**, **FGF**, **PADG**, and **TGF** families (cf. [1], [10], [13], [47]). We next describe the time and space dynamics of one such factor $g(x, t)$ irrespective of its specific biological function which will be considered later on.

To that end we consider our fracture gap $\Omega = (-\frac{L}{2}, \frac{L}{2})$ with $L > 0$ and assume that $g(x, t)$ is released by activated platelets in Ω and freely diffuses within and without Ω . More precisely, we postulate that g satisfies:

$$\frac{\partial g}{\partial t} - D \frac{\partial^2 g}{\partial x^2} + \beta g = \sigma(t)p_a(t)\chi_\Omega \quad \text{for } -\infty < x < \infty, t > 0 \quad (3.40)$$

$$g(x, 0) = 0 \quad \text{for } -\infty < x < \infty \quad (3.41)$$

where $\chi_\Omega(x) = 1$ when x lies in Ω , and $\chi_\Omega(x) = 0$ otherwise. Here D and β denote respectively the diffusion and half-life coefficients of $g(x, t)$. Concerning $\sigma(t)$, we assume it to be of the form:

$$\sigma(t) = \begin{cases} \sigma > 0 & \text{for } T_M < t < T^* \\ 0 & \text{otherwise} \end{cases} \quad (3.42)$$

for some constant σ and some $T^* > 0$. The reason for that choice is that platelets can only release such substances as they had initially stored, since they lack nuclei and hence the possibility to synthesize new molecules.

The linear problem (3.40), (3.41) can be explicitly solved by classical methods to give:

$$g(x, t) = \int_0^t \left(\int_{-L/2}^{L/2} G(x-y, t-s) dy \right) e^{-\beta(t-s)} \sigma(s) p_a(s) ds \quad (3.43)$$

where

$$G(x, t) = \frac{e^{-\frac{x^2}{4Dt}}}{\sqrt{4\pi Dt}} \quad \text{for } -\infty < x < \infty, t > 0. \quad (3.44)$$

Recalling (3.39), for times $T_M < t < T^*$ (3.43) yields:

$$g(x, t) = \sigma P_0 (1 - e^{-\alpha C}) \int_{T_M}^t \left(\int_{-L/2}^{L/2} G(x - y, t - s) dy \right) e^{-\beta(t-s)} ds \quad (3.45)$$

whereas for $t > T^*$:

$$g(x, t) = \sigma P_0 (1 - e^{-\alpha C}) \int_{T_M}^{T^*} \left(\int_{-L/2}^{L/2} G(x - y, t - s) dy \right) e^{-\beta(t-s)} ds \quad (3.46)$$

3.3.4 Recruitment of mesenchymal cells (MSC). Formation of early fibrin-collagen callus (EFC)

Having described the dynamics of a generic growth factor $g(x, t)$ in our previous Section, we now analyze the chemotactic effects induced by growth factors in the population of MSCs and their impact on remodelling the fibrin net to produce a first fibrin-collagen template. We assume that a baseline population of MSC is located at the periosteum, near the fracture border and that when stimulated by $g(x, t)$ such population moves inwards into the fracture gap. When doing so, MSCs eventually become precursors of various cell types instrumental to achieve bone repair. More precisely, let us denote by $m(x, t)$ the concentration of MSCs at a point x at a time t . We postulate that m satisfies:

$$\frac{\partial m}{\partial t} + \frac{\partial}{\partial x} \left(\mu m \frac{\partial g}{\partial x} \right) = 0 \quad ; \quad -\infty < x < \infty, t > T_M \quad (3.47)$$

$$m(x, T_M) = 0 \quad \text{for} \quad -\frac{L}{2} \leq x \leq \frac{L}{2}, \quad (3.48)$$

$$m(x, T_M) = m_0 \quad \text{for} \quad x \leq -\frac{L}{2}, x \geq \frac{L}{2}. \quad (3.49)$$

where $\mu > 0$ is a chemotactic coefficient and m_0 is the concentration of MSC available at the periosteum reservoir. Notice that both diffusive and mitotic effects have been ignored in (3.47). Using (3.45), (3.46) an explicit formula can be obtained for $\frac{\partial g}{\partial x}$. To this end, we note that on setting:

$$\text{erf}(u) = \frac{2}{\sqrt{\pi}} \int_0^u e^{-x^2} dx \quad (3.50)$$

one has that

$$\begin{aligned} I(x, t) &= \int_{-L/2}^{L/2} \frac{e^{-\frac{(x-y)^2}{4Dt}}}{\sqrt{4\pi Dt}} dy \\ &= \frac{1}{2} \left(\operatorname{erf} \left(\sqrt{\frac{T_c}{t}} (1/2 + x/L) \right) + \operatorname{erf} \left(\sqrt{\frac{T_c}{t}} (1/2 - x/L) \right) \right) \end{aligned} \quad (3.51)$$

where

$$T_c = \frac{L^2}{4D}. \quad (3.52)$$

Then there holds:

$$\frac{\partial I}{\partial x}(x, t) = \frac{1}{\sqrt{\pi}} \sqrt{\frac{T_c}{t}} \frac{1}{L} \left(e^{-\frac{T_c}{t}(1/2+x/L)^2} - e^{-\frac{T_c}{t}(1/2-x/L)^2} \right).$$

Setting $\hat{P}_0 = \sigma P_0 (1 - e^{-\alpha C})$ it follows that for $T_M < t < T^*$:

$$\begin{aligned} \frac{\partial g}{\partial x}(x, t) &= \hat{P}_0 \int_{T_M}^t \frac{\partial I}{\partial x}(x, t-s) e^{-\beta(t-s)} ds \\ &= \frac{\hat{P}_0}{\sqrt{\pi} L} \int_{T_M}^t \sqrt{\frac{T_c}{t-s}} \left(e^{-\frac{T_c}{4(t-s)}(1+2x/L)^2} - e^{-\frac{T_c}{4(t-s)}(1-2x/L)^2} \right) e^{-\beta(t-s)} ds. \end{aligned} \quad (3.53)$$

At this juncture it is convenient to make use of non-dimensional variables given by:

$$u = \frac{2x}{L}, \quad \tau = \frac{t-s}{T_c}, \quad \bar{t} = \frac{t-T_M}{T_c} \quad (3.54)$$

Upon introducing (3.54) for times \bar{t} such that $0 < \bar{t} < \frac{T^*-T_M}{T_c}$ (3.53) can be recast in the form:

$$\frac{\partial g}{\partial x}(u, \bar{t}) = \frac{\hat{P}_0 T_c}{\sqrt{\pi} L} \int_0^{\bar{t}} \left(e^{-\left(\frac{1+u}{2\sqrt{\tau}}\right)^2} - e^{-\left(\frac{1-u}{2\sqrt{\tau}}\right)^2} \right) \frac{e^{-T_c \beta \tau}}{\sqrt{\tau}} d\tau \quad (3.55)$$

When $\bar{t} \ll 1$ so is τ , and the integrand in (3.55) is almost zero except for values close to interval boundaries $u = \pm 1$. For instance, when $\bar{t} = 0.01$ a plot for $\frac{\partial g}{\partial x}(u, \bar{t})$ is provided in figure 3.6 below.

When $\bar{t} = O(1)$, that is for times t such that $t - T_M = O(T_c)$, the profile for $\frac{\partial g}{\partial x}(u, \bar{t})$ looks as depicted in Figure 3.7. Such a profile is maintained until it begins to decrease for $t > T^*$. Therefore the main contributions to $\frac{\partial g}{\partial x}$ are achieved for $T_M < t < T^*$,

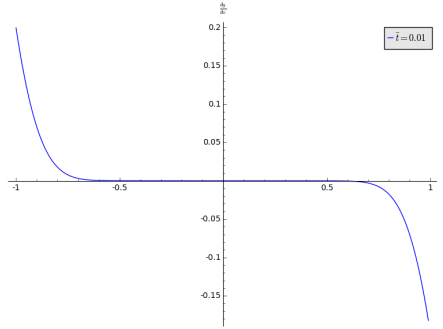


Figure 3.6: The form of $\frac{\partial g}{\partial x}$ for $\bar{t} = 0.01$. All parameters involved are set equal to one for convenience.

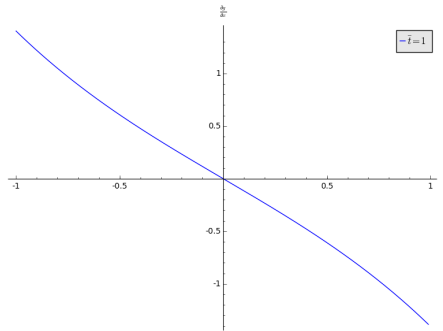


Figure 3.7: A plot of $\frac{\partial g}{\partial x}$ for $\bar{t} = 1$. All parameters involved are set equal to one for convenience.

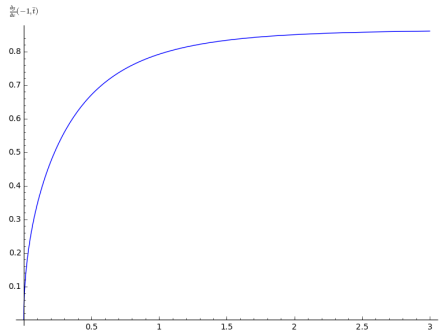


Figure 3.8: A plot of $\frac{\partial g}{\partial x}(-1, \bar{t})$ as a function of \bar{t} , showing quick stabilization to a plateau-like profile. Parameter values as in Figures 3.6 and 3.7.

and are provided by values of u near to the boundary values $u = \pm 1$. For instance, on writing:

$$\frac{\partial g}{\partial x}(-1, \bar{t}) = \frac{\hat{P}_0 T_c}{\sqrt{\pi} L} \int_0^{\bar{t}} \left(1 - \exp\left(-\frac{1}{\tau}\right)\right) \frac{e^{-T_c \beta \tau}}{\sqrt{\tau}} d\tau \quad (3.56)$$

one may obtain a plot for $\frac{\partial g}{\partial x}(-1, \bar{t})$ as a function of \bar{t} that looks as in Figure 3.8:

Note that $\frac{\partial g}{\partial x}(-1, \bar{t})$ quickly saturates to a constant value. Actually, one has that:

$$\begin{aligned} \int_0^{\bar{t}} \left(1 - e^{-\frac{1}{\tau}}\right) \frac{e^{-T_c \beta \tau}}{\sqrt{\tau}} d\tau &\leq \frac{1}{\sqrt{T_c \beta}} \int_0^{\infty} \left(1 - e^{-\frac{T_c \beta}{v}}\right) \frac{e^{-v}}{\sqrt{v}} dv \\ &\leq \frac{1}{\sqrt{T_c \beta}} \int_0^{\infty} \frac{e^{-v}}{\sqrt{v}} dv = \sqrt{\frac{\pi}{T_c \beta}} \end{aligned}$$

Hence:

$$\mu \frac{\partial g}{\partial x}(-1, \bar{t}) \leq \mu \hat{P}_0 \frac{\sqrt{T_c / \beta}}{L} \equiv \mu a, \quad (3.57)$$

and a similar result can be derived at $u = 1$. We are now ready to estimate the time it takes for a front of MSCs to reach the center of the gap at $x = 0$. Once front $x(t)$ has entered into a linear regime (which in particular occurs for times $t - T_M \approx 3T_c$; see Figure 3.8), its equation reads:

$$\begin{aligned} \frac{dx}{dt} &= \mu \frac{\partial g}{\partial x} \\ x(T_M) &= -L/2 \end{aligned} \quad (3.58)$$

Since $\frac{\partial g}{\partial x} \approx -au = -\frac{2ax}{L}$ for $0 < \bar{t} < \frac{T^* - T_M}{T_c}$ and $-\frac{L}{2} < x < 0$, (cf. 3.57) we actually obtain that the differential equation in (3.58) can be approximated by:

$$\frac{dx}{dt} = -\frac{2\mu a}{L} x \quad (3.59)$$

whence

$$x(t) = -\frac{L}{2} e^{-(\frac{2\mu a}{L}(t - T_M))} \quad (3.60)$$

On its turn, the concentration of MSC can be estimated from (3.59) and (3.47), which together yield:

$$\frac{\partial m}{\partial t} - \frac{2a\mu x}{L} \frac{\partial m}{\partial x} = \frac{2a\mu}{L} m \quad (3.61)$$

Thus, if $x(t)$ denotes the characteristic curve of (3.61) starting from $x_0 \leq -\frac{L}{2}$, we obtain from (3.61) that:

$$m(x(t), t) = m_0 e^{\frac{2\mu a}{L}(t - T_M)} \quad (3.62)$$

whereas $m(x(t), t) = 0$ if $x_0 > -\frac{L}{2}$. We may now estimate the time T_F of formation of **EFC** as follows. Due to the approximations made to derive (3.60) the function

$x(t)$ defined there will never reach $x = 0$ in a finite time. We will thus say that **EFC** has been formed when $x(t)$ reaches instead a value $-\varepsilon$ with $0 < \varepsilon \ll 1$ arbitrarily selected. We then may compute T_F from the relation:

$$-\frac{L}{2}e^{-\frac{2\mu a}{L}(T_F - T_M)} = -\varepsilon$$

which gives at once:

$$T_F = T_M + \frac{\sqrt{\beta DL}}{\mu \hat{P}_0} \log\left(\frac{L}{2\varepsilon}\right), \tag{3.63}$$

provided that $T^* > T_F$ (see (3.55)).

We conclude this section by remarking about the negligible impact of diffusion in the process under consideration. To avoid technicalities, we just show here that adding diffusion in (3.47) results in a small correction in the inward motion of **MSC** front. More precisely, let us replace (3.47) by

$$\frac{\partial m}{\partial t} + \frac{\partial}{\partial x} \left(\mu m \frac{\partial g}{\partial x} - D_m \frac{\partial m}{\partial x} \right) = 0 \quad ; \quad -\infty < x < \infty, \quad t > T_M \tag{3.64}$$

where $D_m > 0$ with initial conditions (3.48) (3.49). Using again the approximation $\frac{\partial g}{\partial x} \approx -\frac{2a}{L}x$ in (3.64) the resulting equation can be written in the form

$$\frac{\partial m}{\partial t} - \frac{2\mu a x}{L} \frac{\partial m}{\partial x} - \frac{2\mu a}{L} m - D_m \frac{\partial^2 m}{\partial x^2} = 0 \tag{3.65}$$

We first estimate the characteristic time $\tau_\epsilon^{\text{tr}}$ needed to travel a distance $\frac{L}{2}$ under transport effects. The time to fill an infinitesimal interval of the form $[x - dx, x]$ is given by:

$$\frac{dx}{-2\mu a x/L} = dt.$$

Integrating this expression between $L/2$ and a characteristic size epsilon (ϵ) (which can be interpreted as an intercellular space) we find that $\tau_\epsilon^{\text{tr}}$ satisfies the following relationship:

$$\int_0^{\tau_\epsilon^{\text{tr}}} dt = \int_\epsilon^{\frac{L}{2}} \frac{L}{2\mu a x} dx$$

and then, we have that:

$$\tau_\epsilon^{\text{tr}} = \frac{L}{2\mu a} \log\left(\frac{L}{2\epsilon}\right)$$

Analogously, we estimate the characteristic time $\tau_\epsilon^{\text{diff}}$ for the gap filling due to a diffusion process:

$$\tau_\epsilon^{\text{diff}} \sim \frac{\left(\frac{L}{2} - \epsilon\right)^2}{D_m}$$

Comparing both values of characteristic times we obtain:

$$\frac{\tau^{\text{tr}}}{\tau^{\text{diff}}} = \frac{LD_m}{2\mu a} \frac{\log\left(\frac{L}{2\epsilon}\right)}{\left(\frac{L}{2} - \epsilon\right)^2} \approx \frac{LD_m}{2\mu a} \frac{\log\left(\frac{L}{2\epsilon}\right)}{\left(\frac{L}{2}\right)^2} = \frac{2D_m}{\mu a L} \log\left(\frac{L}{2\epsilon}\right)$$

Assuming a value of ϵ of $\frac{L}{100}$, then we can estimate the quotient (let us recall that $L = 2$ mm):

$$\frac{\tau^{\text{tr}}}{\tau^{\text{diff}}} = \frac{2D_m}{\mu\alpha L} \log\left(\frac{L}{2\epsilon}\right) = \frac{2 * 10^{-6}}{0.5 * 10^{-2} * 1.25 * 0.2} \log(50) \approx 6 \cdot 10^{-3}$$

which confirms the low impact of diffusion in the process under consideration, showing that the transport effects occur in a much shorter characteristic time than diffusive ones.

3.4 A sequence of times

We now briefly discuss on the comparative values of the characteristic times obtained in our previous sections. To begin with, we observe that a correct timing of the overall process requires that

$$T_M < T_f < T_c < T_F < T^* \quad (3.66)$$

where T_M , T_f , T_c , T_F , and T^* have been respectively defined in (3.3), (3.21), (3.52), (3.63) and (3.42). For simplicity, we take $T_M = 0$ in the sequel, since hematoma formation is known to begin shortly after fracture. On the other extreme, it is reasonable to select T^* of the order of the average platelet life-span, so that we may take:

$$T^* \approx 10 \text{ days} \quad (3.67)$$

(cf. [33]). To estimate the values of the remaining times in (3.66) is in principle feasible by means of the corresponding formulas obtained. However, while some of the parameters appearing there can be reasonably guessed (at least from in vitro experiments), little can be said about parameters as α and σ appearing in (3.37) and (3.40) respectively. We next describe the type of information on the sequence of times in (3.66) that can be obtained under current uncertainty constraints.

To begin with, consider the value obtained in (3.21) for T_f . In the earliest detectable stages in fibrin clot formation, when fragmentation and deactivation effects are ignored, the value of T_f can be compared with the prothrombin time T_p , a parameter routinely measured in blood tests [4]. T_p is measured in decalcified plasma where platelets have been removed, and a typical value obtained is $T_p \approx 10$ seconds. If we compare the fastest estimate for T_f obtained in Section 3.2 (see (3.21)), we should have:

$$T_f = \frac{1}{8F_M k_p (1 - e^{-k_g C})} \approx 10 \text{ sec} \quad (3.68)$$

F_M in (3.68) is commonly estimated in blood tests. A typical value for F_M is

$$F_M \approx 3 \text{ gr/1} = 9000 \text{ nM} \quad (3.69)$$

(see [26]). Fibrin polymerization rates seem to have been reported only in vitro ([26] and references therein). For instance, we may take

$$k_p = 4 \times 10^{-3} \text{ (nM} \cdot \text{min)}^{-1} \quad (3.70)$$

(cf. [58]). One then readily sees that $8F_M k_p \approx 4.8 \text{ (sec)}^{-1}$. Then estimate (3.68) follows provided that

$$1 - e^{-k_g C} = \frac{1}{48} \quad (3.71)$$

which holds provided that $k_g C \approx 0,0211$. As a matter of fact, values for k_g have been reported ([58], [26]). For instance, it has been suggested that

$$k_g = 3 \times 10^{-4} \text{ (nM} \cdot \text{min)}^{-1} \quad (3.72)$$

(cf. [58]). From (3.71) and (3.72) we obtain that under such assumptions

$$C \approx \frac{10^4}{3} 0.0211 \text{ nM} \cdot \text{min} = 0.47 F_M \text{ sec} \approx \frac{F_M}{2} \text{ sec}. \quad (3.73)$$

It has to be stressed that, as remarked in Section 2, the time to develop a mature fibrin clot is considerably larger than the value provided in (3.68). Indeed, to keep track of the actual unfolding of a fibrin net, quantities other than the prothrombin time are measured in clinical practice [46]. Examples are the clotting time, CT, defined as the time required for blood to form a initial clot from a given volume of blood in a glass tube, which usually ranges between 5 to 15 minutes, and the retraction time RT, defined as the time taken for a blood sample to become solid enough so that it could separate from the walls of a crystal vessel where coagulation is taking place, and that ranges between 1 to 2 hours. As a matter of fact, times as those reported for CT or RT can be obtained from our formulas (3.21) or (3.25) by selecting C and k_b in a suitable manner there.

Consider now T_c given in (3.52) through the relation

$$T_c = \frac{L^2}{4D} \quad (3.74)$$

where D is the diffusion coefficient of the growth factor considered. Since not much seems to be known about in vivo values for D , we may now try on (3.74) a typical diffusivity value, say $D = 10^{-6} \text{ cm}^2/\text{sec}$. Taking now $L = 2 \text{ mm}$ (see Appendix A) we obtain:

$$T_c = 10^4 \text{ sec} \approx 3 \text{ hours} \quad (3.75)$$

Notice that by (3.68) and (3.75), $T_f \ll T_c$. Moreover, a slower diffusivity will result in an increased value of T_c according to (3.74).

Let us now remark on T_F , the time required for early callus formation, for which we have obtained estimate (3.63) in Section 3.4. For definiteness, let us take $\varepsilon = \frac{e^{-N}}{2}$ for some integer N there. Or taking N such that $N \gg \log(L)$, we see that

$$T_F \approx \frac{\sqrt{\beta D L N}}{\mu \sigma P_0 (1 - e^{-\alpha C})} \quad (3.76)$$

Some of the parameters in (3.76) are known within reasonable ranges. For instance, values for half-lives of growth factors have been reported in the literature, although

they considerably differ from one reference to another. For definiteness we take here $\beta = 6 \cdot 10^{-4} \text{ (min)}^{-1}$ [3]. Keeping to our previous choices $L = 2 \text{ mm}$ and $D = 10^{-6} \text{ cm}^2/\text{sec}$, and selecting $N = \frac{50}{\sqrt{6}}$ we deduce that $\sqrt{\beta D L N} \approx 10^{-4} \text{ cm}^2/\text{sec}$. Platelet counts are commonly made in blood tests, with values ranging between $1.5 \cdot 10^5$ to $40 \cdot 10^5$ units per cubic millimeter, and mean platelet weight has been estimated to be about 10 picograms [34]. We therefore may take $P_0 = 2\text{gr/liter}$ as a reference value. On the other hand, the chemotactic coefficient μ has been measured for neutrophils in some experimental settings [56] where values as $400 \text{ cm}^2/(\text{M} \cdot \text{sec})$ have been reported. Just for comparison purposes, we may consider here growth factor concentrations in the previous estimate for μ so that $\mu P_0 = 10^{-5} \text{ cm}^2/\text{sec}$. In this manner we will obtain:

$$\frac{\sqrt{\beta D L N}}{\mu P_0} \simeq 10 \quad (3.77)$$

Concerning the remaining parameters in (3.76) it is natural to assume $\sigma = O\left(\frac{1}{T^*}\right)$ where T^* is given in (3.67). On taking $\sigma = \frac{1}{T^*}$ and selecting then the conversion factor $1 - e^{-\alpha C} \simeq \frac{1}{50}$, we would eventually arrive at

$$T_F \simeq \frac{T^*}{5} \simeq 2 \text{ days} \quad (3.78)$$

Needless to say, our previous estimates have to be considered as very preliminary. For instance, for times of the order of CT or RT, additional characteristic times of the various coagulation and fibrinolytic networks involved need to be investigated. Actually, CT is used as part of hemophilic test, so that the dynamics of individual coagulation factors as FVIII need to be accounted for there. On the other hand, once the fibrin clot has been formed (which begins to occur quite fast; see [5]) the half life of growth factors can be extended due to their anchorage in such a net ([49], [60]). Actually, (3.76) suggests that an increase in that value from β to 4β would result in doubling the corresponding value in (3.76). This effect, however, can be somehow compensated by the slowdown in diffusivity D as the medium becomes denser.

3.5 Concluding remarks

In this work we have used mathematical models to explore the early stages of bone fracture repair. Bone health is essential to ensure high quality of human life, and its significance becomes even more important in aging societies, as many developed countries are. Human bone has an impressive capability for self-repair. In fact, human skeleton is constantly being remodelled, and as we have already noticed at the Introduction, bone microfractures induced by exercise are routinely self-healed without being ever noticed [6]. It has been observed that such repairing mechanisms repeat many processes present at the developmental program that drives ossification during the embryonic stage [18], [19]. Moreover, bone repair has some common features with other tissue repairing processes as wound healing [32], [52]. It follows from these remarks that each improvement in our understanding of the process of

bone self-repair may have significant consequences, and it is widely expected that quantitative models of bone healing may provide valid contributions to that end.

However, as in many other biological processes, when faced with the goal of providing mathematical models for bone repair, one has to confront a significant obstacle. More precisely, while many of the key agents in the process under consideration have been identified, little is known concerning the precise manner whereby these agents coordinate themselves to achieve bone repair. For instance, only partial information seems to be available on the detailed network hierarchy of the corresponding biochemical cascades, and precise information on the order and rate constants of the chemical reactions involved in cell signalling during that process remain largely unknown. This leaves few options except selecting ad hoc such parameters when it comes to carry out simulations to recover observed behaviours. However, it is well known that a given dynamics can be recovered from different sets of parameter values, so that the insight gained through extensive parameter fitting has to be carefully weighted ([29], [22]).

Bearing these remarks in mind, we have aimed in this work at discussing simple models that could however provide some information into the specific issue addressed, namely the timing of events taking place at the early stages of bone fracture repair. Specifically, we restrain our attention to processes unfolding from bone break up until the formation of a first fibrous callus that, upon suitable remodelling, will lead to successful bone repair. While comparatively simple when compared with later stages (for instance, mechanical effects do not play yet so relevant a role as in posterior bone remodelling), we already deal here with some of the main processes that will be at work later on, as chemotactic recruitment of **MSCs** (mesenchymal stem cells). **MSCs** will thus divide and differentiate to produce cell lineages whose interaction with previous elastic scaffolds will eventually lead to complete fracture healing. Actually, the formation of the first (and crucial) such scaffold (a fibrin net) is addressed in detail here, and its onset is kept track of and characterized as the unfolding of a sol-gel phase transition.

Concerning the simplicity of our models, a few words are in order. When dealing with any of the processes considered, we have attempted to focus on the main features needed to derive the sought-for information, namely the time it takes for such a process to develop. When doing so, we have considered effective processes, where in particular various biochemical cascades have been lumped into a single equation, rather than exploring the intricacies of each aspect involved. Our approach is illustrated by our discussion on thrombin-induced fibrin polymerization in Section 3.1, where further remarks on the issues addressed can be found.

As a consequence of our work, some estimates for what we retain to be the main characteristic times of the earliest stages considered have been obtained. These have been summarized and estimated in Section 3 and 4 following a brief survey on the main underlying biological aspects which makes the content of Section 2. We have discussed in section 4 how meaningful estimates for such characteristic times can be provided, even in the presence of large parameter uncertainty, when our model is compared with experimental data. However, additional work is required to improve

the form of the estimates therein derived. Particularly, we have selected for that purpose the induction of thin fractures in rats, for which a number of experiments have been performed (for the corresponding experimental set up, see Appendix A). Finally, while keeping models as simple as possible, we have succinctly discussed on a number of possible extensions of the results obtained, as for instance the case where thrombin sources are spatially distributed in Section 3.1, or a justification of the negligible nature of diffusion aspects in the chemotactic recruitment of MSCs during early callus formation in Section 3.4. Other aspects, however, will require of a more detailed analysis. A particularly relevant example of the latter is the evaluation of the robustness and redundancy properties induced by the simultaneous action of several growth factors with partially overlapping functions. We intend to address this and other related issues in future work.

Bibliography

- [1] Anitua, E., Andia, I., Ardanza, B., Nurden, P., Nurden, A.: Antologous platelets as a source of proteins for healing and tissue regeneration. *Thromb. Haem.* **91**(1), 4–15 (2004)
- [2] Ayati, B., Edwards, C., Webb, G., Wilswo, J.: A mathematical model of bone remodelling dynamics for normal bone cell populations and myeloma bone disease. *Biology Direct* **5** (2010). <http://www.biology-direct.com/content/5/1/28>
- [3] Beenken, A., Mohammadi, B.: The fgf family: Biology, pathophysiology and therapy. *Nat. Rev Drug. Discover.* **8**(3), 235–253 (2009)
- [4] Van den Besselaar, A.M.: Precision and accuracy of the international normalized ratio in oral anticoagulant control. *Haemostasis.* **26**(2s), 248–265 (1996)
- [5] Bolander, M.: Regulation of fracture repair by growth factors. *Proc Soc Exp Biol Med* **200**, 165–170 (1992)
- [6] Boyde, A.: The real response of bone to exercise. *J. Anat* **203**(2), 173–189 (2003)
- [7] Brass, L.: Thrombin and platelet activation. *Chest* **124**(3), 185–255 (2003)
- [8] Butenas, S., Vant Veer, C., Mann, K.: Normal thrombin generation. *Blood* **94**(7), 2169–2178 (1999)
- [9] Chung, R., Cool, J., Scherer, M., Foster, B., Xian, C.: Roles of neutrophil-mediated inflammatory response in the bony repair of injured growth plate cartilage in young rats. *J. Leukoc. Biol* **80**, 1272–1280 (2006)
- [10] Cicha, I., Garlich, C., Daniel, W., Goppelt-Struebe, M.: Activated human platelets release connective tissue growth factor. *Throm. Haem.* **91**(4), 755–760 (2004)

- [11] Colnot, C., Huang, S., Helms, J.: Analyzing the cellular contribution of bone marrow to fracture healing using bone marrow transplantation in mice. *Biochem. Biophys Res Commun* **350**, 557–561 (2006)
- [12] Danforth, C., Orfeo, T., Mann, K., Brummel?Ziedins, K., Everse, S.: The impact of uncertainty in a blood coagulation model. *Math. Med. Biol.* **4**, 323–336 (2009)
- [13] Dimitriou, R., Tsiridis, E., Giannoudis, P.: Current concepts of molecular aspects of bone healing. *Injury Int. J. Care.* **36**, 1392–1404 (2005)
- [14] Eghbali-Fatourehchi, J., Lamsam, D., Fraser, D., Nagel, B., Riggs, S., Khosla: Circulating osteoblast-lineage cells in humans. *N Engl J Med.* **352**, 1959–1966 (2005)
- [15] Einhorn, T.: The cell and molecular biology of fracture healing. *Clin.Orthop.Relat. Res* **355**(S), 7–21 (1998)
- [16] Fasano, A., Herrero, M., Lopez, J., Medina, E.: On the dynamics of the growth plate in primary ossification. *Journal Theor. Biol* **265**, 543–553 (2010). doi: 10.1016/j.jtbi.2010.05.030
- [17] Fasano, A., Santos, R., Sequeira, A.: Blood coagulation: a puzzle for biologists, a maze for mathematicians. In: *Modelling Physiological Flows*, pp. 44–76. Springer Verlag (2011)
- [18] Ferguson, C., Miclau, T., Alpern, E., Helms, J.: Does adult fracture repair recapitulate embryonic skeletal formation? *Mech. Dev.* **87**, 57–66 (1999)
- [19] Ferguson, C., Miclau, T., Hu, D., Alpern, E., Helms, J.: Common molecular pathways in skeletal morphogenesis and repair. *Ann. New York Acad. Sci.* **857**, 33–42 (1988)
- [20] Gerstenfeld, L., Alkhiary, Y., Krall, E., Nicholls, F., Stapleton, S., Fitch, J., Bauer, M., Kayal, R., Graves, D., Jepsen, K., Einhorn, T.: Three-dimensional reconstruction of fracture callus morphogenesis. *J HistochemCytochem* **54**, 1215–1228 (2006)
- [21] Gerstenfeld, L., Cullinane, D., Barnes G.L.and Graves, D., Einhorn, T.: Fracture healing as a post-natal developmental process: molecular, spatial, and temporal aspects of its regulation. *J Cell Biochem* **88**, 873–884 (2003)
- [22] Ginzburg, L.R., Jensen, C.X.J.: Rules of thumb for judging ecological theories. *Trends in ecology and evolution.* **19**(3), 121–126 (2004)
- [23] Graham, J., Ayati, B., Holstein, S., Martin, J.: The role of osteocytes in targeted bone remodelling: a mathematical model. *PLoSOne* **22**(8(5e63884)) (2013). doi: 10.1371/journal.pone.0063884

- [24] Groothuis, A., Duda, G., Wilson, C., Thompson, M., Hunter, M., Simon, P., Bail, H., van Scherpenzeel, K., Kasper, G.: Mechanical stimulation of the pro-angiogenic capacity of human fracture haematoma: involvement of vegf mechano-regulation. *Bone* **47**, 438–444 (2010)
- [25] Guria, G., Herrero, M., Zolobina, K.: A mathematical model of blood coagulation induced by activation sources. *Discrete and Continuous Dynamical Systems* **25**(1), 175–194 (2009)
- [26] Guria, G.T., Herrero, M.A., Zlobina, K.E.: Ultrasound detection of externally induced microthrombi cloud formation: a theoretical study. *J. Eng. Math.* **66**, 293–310 (2010)
- [27] Guria, K., Gagarina, A., Guria, G.: Instabilities in fibrinolytic regulatory system. theoretical analysis of blow-up phenomena. *J. Theor. Biology* **304**, 27–38 (2012)
- [28] Guy, R., Fogelson, A., Keener, J.: Fibrin gel formation in a shear flow. *Math. Med. Biol.* **24**, 111–130 (2007)
- [29] Hemker, H.C., Kerdelo, S., Kremers, R.M.W.: Is there value in kinetic modelling of thrombin generation? *J. Thromb. Haemost.* **10**, 1470–1477 (2012)
- [30] Hollinger, J., Onikepe, A., MacKrell, J., Einhorn, T., Bradica, G., Lynch, S., Hart, C.: Accelerated fracture healing in the geriatric, osteoporotic rat with recombinant human platelet-derived growth factor-bb and an injectable beta-tricalcium phosphate/collagen matrix. *J Orthop Res* **26**, 83–90 (2008)
- [31] Hughes, S., Hicks, D., OKeefe, R., Hurwitz, S., Crabb, I., Krasinskas, A., Loveys, L., Puzas, J., Rosier, R.: Shared phenotypic expression of osteoblasts and chondrocytes in fracture callus. *J Bone Miner Res* **10**, 533–544 (1995)
- [32] Javierre, E., Vermolen, F., Vuik, C., Van der Zwaag, S.: A mathematical analysis of physiological and morphological aspects of wound closure. *J. Math. Biol* **59**, 605–633 (2009). doi: 10.1007/s 00285-008-0242-7
- [33] Kameth, S., Blann, A.D., Lip, G.Y.H.: Platelet activation: assesment and quantificaion. *European Hearth J.* **22**, 1561–1571 (2001)
- [34] Kiem, J., Borberg, H., Iyengar, G.V., et al.: Water content of normal human platelets and measurements of their concentrations og cu, fe, k and zn by neutron activation analysis. *Clin. Chem.* **21**(5), 705–710 (1979)
- [35] Komarova, S., Smith, R., Dixon, J., Sims, S., Wahl, L.: Mathematical model predicts a critical role for osteoclast autocrine regulation in the control of bone remodelling. *Bone* **33**, 206–215 (2003). doi: 10.1016/S8756-3282(03)00157-1
- [36] Malizos, N., Papatheodorou, L.: The healing potential of the periosteum. molecular aspects. *Injury* **36**(S3), S13–S19 (2005)

- [37] Mann, K., Butenas, S., Brummel, K.: The dynamics of thrombin formation. *Arteriosclerosis Thrombosis and Vascular Biology* **23**, 17–25 (2003)
- [38] Mc Dougall, S., Dallon, J., Sherratt, J., Maini, P.: Fibroblast migration and collagen deposition during termal wound healing: mathematical modelling and clinical implications. *Phil. Trans. Roy. Soc* **364**, 1385–1405 (2006). doi: 10.1098/rsta.2006.1773
- [39] McKibbin, B.: The biology of fracture healing in long bones. *J. Bone Joint Surg.B* **2**(60), 151–162 (1978)
- [40] Moore, S., Saidel, G., Knothe, U., Knothe Tate, M.: Mechanistic , mathematical model to predict the dynamics of bone defects via mechanical feedback and mediation of biochemical factors. *PLoS Comp. Biol* **10**(6e1003604) (2014). doi: 10.1371/journal.pcbi.1003604
- [41] Moreo, P., Garcia Aznar, J., Doblare, M.: Bone ingrowth on the surface of endosseous implants. part i: mathematical model. *J. Theor. Biol* **260**, 1–12 (2009)
- [42] Murphy, K., Hall, C., Maini, P., Mc Cue, S., Sean Mc Elwain, D.: A fibrocontractive mechanochemical model of wound closure incorporating realistic growth factor kinetics. *Bull. Math. Biol* **74**, 1143–1170 (2012). doi: 10.1007/s11538-011-9712-y
- [43] Orfeo, T., Butenas, S., Brummel-Ziedins, K., Mann, K.: The tissue factor requirement in blood coagulation. *J. Biol. Chemistry* **280**(52), 42,887–42,896 (2005)
- [44] Pivonka, P., Dunstan, C.: Role of mathematical modeling in bone fracture healing. *BioKEyReports* **1**(221) (2012). doi: 10.1038/bonekey 2012.221
- [45] Prokharau, P., Vermolen, F., Garcia-Aznar, J.: Model for direct bone apposition on a pre-existing surface during peri implant osteointegration. *J. Theor. Biol* **304**, 131–142 (2012)
- [46] Rodak, B.F., Fritsma, G.A., Keohane, E.: *Hematology: Clinical Principles and Applications.*, 4 edn. Saunders, USA. (2011)
- [47] Rozman, P., Boita, Z.: Use of platelet growth factor in treating wounds and soft-tissue injuries. *Acta. Dermat.* **16**(4), 156–165 (2007)
- [48] Rumi, M., Deol, G., Singapuri, K., V.D., P.J.: The origin of osteo- progenitor cells responsible for heterotopic ossification following hip surgery: an animal model in the rabbit. *J Orthop Res.* **23**, 34–40 (2005)
- [49] Sahni, A., Francis, C.W.: Vascular endothelial growth factor binds to fibrinogen and fibrin and stimulates endothelial cell proliferation. *Blood* **96**, 3772–3778 (2000)

- [50] Schmidt-Bleek, K., Schell, H., Schulz, N., Hoff, P., Perka, C., Buttgerit, F., Volk, H., Lienau, J., Duda, G.: Inflammatory phase of bone healing initiates the regenerative healing cascade. *Cell Tissue Res* **347**, 567–573 (2012)
- [51] Shapiro, F.: Bone development and its relation to fracture repair. the role of mesenchymal osteoblasts and surface osteoblasts. *Eur Cells Mater.* **15**, 53–76 (2008)
- [52] Sonnemann, K.J., Bement, W.M.: Wound repair: toward understanding and integration of single cell and multicellular wound responses. *Ann. Rep. Cell and Develop Biol.* **27**, 237–263 (2011)
- [53] Stockmayer, W.: Theory of molecular size distribution and gel formation in branched-chain polymers. *J.Chem. Physics* **11**(2), 45–55 (1943)
- [54] Street, J., Winter, D., Wang, J., Wakai, A., McGuinness, A., Redmond, H.: Is human fracture hematoma inherently angiogenic? *Clin Orthop* **378**, 224–237 (2000)
- [55] Takahara, M., Naruse, T., Takagi, M., Orui, H., Ogino, T.: Matrix metalloproteinase-9 expression, tartrate-resistant acid phosphatase activity, and dna fragmentation in vascular and cellular invasion into cartilage preceding primary endochondral ossification in long bones. *J Orthop Res.* **22**, 1050–1057 (2004)
- [56] Tranquillo, R.T., Zigmund, S.H., Lauffenburger, D.A.: Measurement of the chemotaxis coefficient for human neutrophils in the under-agarose migration assay. *Cell Motility and Cytoskeleton* **11**, 1–15 (1988)
- [57] Wagenwood, R., Hemker, P.W., Hemker, H.C.: The limits of simulation of the clotting system. *J. Thromb. Haemost.* **4**, 1331–1338 (2006)
- [58] Weisel, J.W., Veklich, Y., Gorkun, O.: The sequence of cleavage of fibropeptides from fibrinogen is important for protofibrin formation and enhancement of lateral aggregation. *J. Mol. Biol.* **232**, 285–297 (1993)
- [59] Wiltzius, P., Dietler, G., Kanzig, W., Haberli, A., Straub, P.: Fibrin polymerization studied by static and dynamic light scattering as a function of fibrinopeptide a release. *Biopolymers* **21**, 2205–2223 (1982)
- [60] Yon, Y.R., Won, J.E., Jeon, E., et al.: Fibroblast growth factors: biology, function and applications for tissue engineering. *J. Tissue Eng.* **1** (2010)
- [61] Yoo, J., Johnstone, B.: The role of osteochondral progenitor cells in fracture repair. *Clin. Orthop. Relat. Res.* **3**(55), S73–S81 (1998)

Details of computer simulations of the model of BMU operation during bone remodeling

A.1 Time evolution of the BMU

- **Initialization:** Simulations take place in a two-dimensional cellular automata (CA) of 150 x 250 boxes. 125 rows of this matrix are initially occupied by bone matrix and the rest by bone marrow. A row of OBL lies in the interface between them. OCYs are initially located at fixed, regularly spaced positions within the bone matrix. A random perturbation is then applied to their positions to avoid any potential effect of symmetries on the simulations of the model. At this point, OCYs and OBLs release signals that diffuse through the bone matrix until an equilibrium is attained. This equilibrium is determined by the balance between signal production and decay. In this moment, a region of OCY apoptosis is randomly defined within *a priori* defined boundaries (*Depth* := maximum depth and *Width* := maximum width).

- **Time evolution:**

Simulations of the model occur in discrete time steps of length $\Delta t = 0.01$. The input for an iteration of the model corresponding to time $t = t_0$ includes a set of vectors (one for each of the cells coexisting in the model at that time) with the coordinates of the box occupied by the cell, and its state variables (amount of inhibitory molecules).

1.- OBL

The state variable considered in the model for the i -th OBL is the amount of activation inhibitor d_{B_i} . The corresponding vector is:

$$v_{B_i}(t_0) = \{(x, y), d_{B_i}(t_0)\}$$

2.- OBA

For each OBA there are three different inhibitory molecules, namely c_A , d_A and a_A , blocking cell division, differentiation and apoptosis. The state vector for the i -th OBA is:

$$v_{A_i}(t_0) = \{(x, y), \{c_{A_i}(t_0), d_{A_i}(t_0), a_{A_i}(t_0)\}\}$$

3.- OPL

Differentiation of OPL into OCL is controlled by the inhibitor d_P , so that the state vector of the i -th OCP is given by:

$$v_{P_i}(t_0) = \{(x, y), d_{P_i}(t_0)\}$$

4.- OCL

Active osteoclast can die by apoptosis and dig into old bone. The state vector for the i -th OCL includes the amount of apoptosis inhibitor a_{C_i} and the amount of old bone b_{C_i} at the box occupied by the OCL:

$$v_{C_i} = \{(x, y), \{a_{C_i}(t_0), b_{C_i}(t_0)\}\}$$

Input also includes the values of signals S , T and R at each box of the CA.

The first step of each iteration consists in the definition of a system of ordinary differential equations that describe the dynamics of the state variables (see Section 2). It consists of $N_B(t_0) + 3 \times N_A(t_0) + N_P(t_0) + 2 \times N_C(t_0)$ equations, where N_B , N_A , N_P and N_C are the number of OBL, OBA, OCP and OCL at time t_0 respectively. The system is then solved numerically using the explicit Runge-Kutta method implemented in the function `NDSolve` of Mathematica (Wolfram Research, Inc., Mathematica, Version 9.0, Champaign, IL).

If neither the amount of bone at a box occupied by a OCL or some of the inhibitors goes to zero during a time step the state of signals S , R and T is actualized and the model moves to the next time step. Alternatively, the model displays different behaviors depending on what variable (or variables) have gone to zero:

1.- OBLs activation inhibitor (d_B)

This corresponds to the activation of one or more OBLs. In this case, the activated OBL are removed from the list of cells of the model, and their positions in the CA are occupied by newly formed OBAs.

2.- OBAs division inhibitor (c_A)

OBAs form a continuous layer of cells that progresses into the cutting cone created by OCL. By construction, only OBAs that are not located in boxed adjacent to bone can divide. Moreover, OBA division can only occur if some of the OBA are not attached to bone yet. In case of OBA division, the position of OBAs is recalculated as summarized in Figure A1.

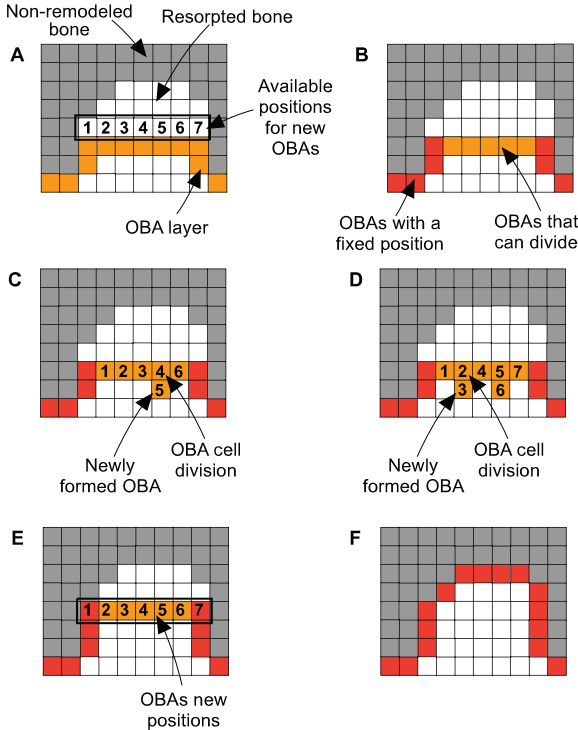


Figure A.1: **Movement of OBAs after cell division.** **A)** The layer of OBAs (in orange) is adjacent to old bone (in grey). There are 7 available positions for new OBAs marked with a thick black line. **B)** OBAs attached to the bone surface (in red) can neither divide nor move. **C)** In case of cell division, one new OBA appears. In the case depicted in the figure there are 6 OBAs after cell division that can move, and 7 free positions, so the layer of OBAs cannot progress into the resorpted bone. The new OBA is located in a cell adjacent to that of the dividing OBA. **D)** After a new cell division there are 7 OBA free to move, so the front of OBA can occupy the next set of available positions as shown in **E).** **E)** OBAs that reach a position adjacent to bone (OBAs labelled with 1 and 7 in red) remain fixed and do not divide. **F)** When all OBAs are attached to the bone surface cell division is no longer possible. From this moment, OBAs start to secrete osteoid matrix, can undergo apoptosis and move downwards.

3.- OBAs apoptosis and differentiation inhibitors (a_A and d_A)

During the bone formation stage, OBAs form a continuous layer of cells that fills the cutting cone created by OCL with new osteoid matrix. Apoptosis of OBAs and differentiation into OCY entail the movement of the OBA layer into the empty cutting cone as described in Figure A.2. In case of differentiation, the OBA is replaced by a new OCY in the same box.

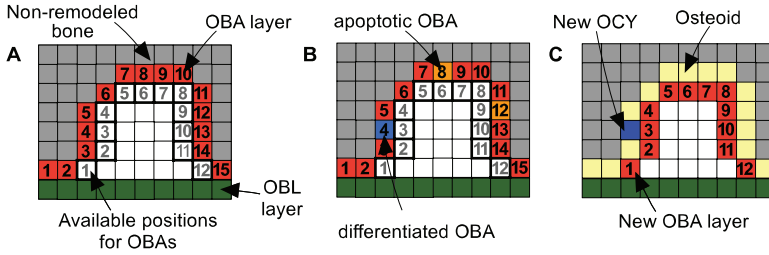


Figure A.2: **Movement of OBAs after apoptosis and differentiation.** **A)** A layer of 15 OBAs (in red) is adjacent to the bone matrix. There are 12 available positions for the new layer of OBAs, marked with a thick black line. New positions are bounded by the layers of OBAs and OBLs. **B)** In this moment, the number of apoptotic (8 and 12, in orange) and differentiated (4, in blue) OBAs equals the difference between the current number of OBAs (15) and the number of available positions (12), so that the layer of OBAs can move. **C)** Boxes that were occupied by OBAs in the previous stage are now filled with osteoid (yellow). A new OCY is placed in the box where an OBA has differentiated.

4.- OCPs differentiation inhibitor (d_P)

OCPs are located adjacent to the layer of OBLs. In case of activation, the corresponding OCP is replaced by a newly formed OCL that moves to the closed box within the bone matrix that is not occupied by any other cell.

5.- OCLs apoptosis inhibitor (a_C)

OCLs whose apoptosis inhibitor disappears are removed from the set of cells in the model for the next iteration.

6.- Bone removal by OCPs (b_P)

OCLs remove old bone from the box where they are located according to equation [1]. When the amount of bone goes to zero, the OCL moves to one of the unoccupied adjacent boxes in the bone matrix. The OCL chooses the box with the highest amount of S signal that is farther from the OBL layer.

After cell fate choices, the set of cells and the amounts of signals S , T and R are updated and the model starts a new iteration.

• **End of the simulation:**

Simulations end when the bone remodeling process is completed (old bone has been replaced by new osteoid matrix) and a new equilibrium (for signals S and

T) has been reached.

A.1.1 Pseudo-code guidelines

Input parameters

t_{max} := maximum duration of simulations

$Depth$:= maximum depth of the apoptosis region

$Width$:= maximum width of the apoptosis area

$bone(x, y)$:= 1 if the box is occupied by bone at initial time and 0 otherwise

$position(OCY, 0)$:= initial position of OCYs

$position(OBL, 0)$:= initial position of OBLs

$position(OCF, 0)$:= initial position of OCFs

Structural parameters

α_k^h := effect of external signals of type h on the dynamics of inhibitors in cells of type k

D_B := maximum amount of inhibitor d_B that can accumulate inside a OBL

$dp_h(d)$:= diffusion profile of signal h as a function of distance d

γ_h := rate of decay of signal of type h

Variable parameters

$\{a_{k0}, d_{k0}, c_{k0}\}$:= amount of inhibitors in newly formed cells of type k

δ_A Distance of OCY inhibition of OBA differentiation

Q_k^h := rate of production of signal of type h by cells of type k

Initialization

- 1 Input the bone matrix $bone(x, y)$
- 3 Input and the boxes occupied by OCY, OBL and OCL.
- 4 Diffusion and decay of signals S and T until equilibrium
- 5 Define a random region of OCY apoptosis
- 6 Set $t := 0$
- 7 **REPEAT**
 - 8 Input the set of positions and state variables of all cells
 - 9 Input the amount of signals S , T and R at each box of the CA

- 10 Write the system of ODEs that describe the dynamics of the state variables as functions of the external signals
- 11 **REPEAT**
 - 12 Numerical integration of the systems of ODEs for a time step Δt
 - 13 Diffusion and decay of signals S , T and R during the time step Δt
 - 14 set $t = t + \Delta t$
- 15 **UNTIL** some state variable goes to zero
- 16 If $(d_{Bi}(x, y; t) \leq 0)$ then remove the i -th OBL and add a new OBA at box (x, y)
- 17 If $(c_{Ai}(x, y; t) \leq 0)$ then
 - 18 add a new OBA at a box adjacent to (x, y)
 - 19 recalculate OBAs positions
- 20 If $(a_{Ai}(x, y; t) \leq 0)$ then
 - 21 remove the i -th OBA
 - 22 recalculate OBAs positions
 - 23 If (change in OBAs position) then fill old positions with osteoid
- 24 If $(d_{Ai}(x, y; t) \leq 0)$ then
 - 25 remove the i -th OBA
 - 26 add a new OCY at (x, y)
 - 27 recalculate OBAs positions
 - 28 If (change in OBAs position) then fill old positions with osteoid
- 30 If $d_{Pi}(x, y; t) \leq 0$ then
 - 31 remove the i -th OCP
 - 32 add a new OCL at the box of the bone matrix closest to (x, y)
- 33 If $a_{Ci}(x, y; t) \leq 0$ then remove the i -th OCL
- 34 If $b_{Bi}(x, y; t) \leq 0$ then
 - 35 set $bone(x, y) = 0$
 - 36 move the OCL to a new position in the bone matrix
- # We remark that several cell decisions can take place simultaneously
- 37 **UNTIL** the end of bone remodeling process

Parameter	Description	Value
$(Depth, Width)$	Maximum depth and width of the OCY apoptosis region	(80, 80)
d_{B0}	Initial amount of differentiation inhibitor in newly formed OBLs	3
D_B	Maximum amount of differentiation inhibitor in OBLs	4
$(\alpha_B^{S_1}, \alpha_B^{S_1})$	OBL structural parameters	(1, 1)
(c_{A0}, a_{A0}, d_{A0})	Initial amount of inhibitors in newly formed OBA	(1.5, 5, 2)
$(\alpha_A^T, \alpha_A^{S_1}, \alpha_A^{S_2}, \alpha_A^{S_3}, \alpha_A^{S_4})$	OBA structural parameters	(0.01, 0.6, 15, 1)
δ_A	Ratio of OCY inhibition of OBA differentiation	1
d_{P0}	Initial amount of differentiation inhibitor in OCP	0.5
(α_P^R, α_P^S)	OCP structural parameters	(3, 5)
a_{C0}	Initial amount of apoptosis inhibitor in OCL	1
$(\alpha_C^{S_1}, \alpha_C^{S_2}, \alpha_C^{S_3}, \alpha_C^{S_4})$	OCL structural parameters	(2, 2.5, 2, 6)
$(dp^S(d), dp^T(d), dp^R(d))$	Diffusion profile of signals S, T and R	$dp^S(d) = dp^T(d) = dp^R(d) = \text{Max}(0, 4 - d)$
$(\gamma_S, \gamma_T, \gamma_R)$	Decay rates of signals S, T and R	(0.01, 0.01, 0.01)
(Q_Y^S, Q_Y^T)	Rates of production of signals S and T by OCYs	(10, 1)
Q_B^T	Rate of production of signal T by OBL	2
(Q_A^T, Q_A^R)	Rates of production of signals T and R by OBAs	(1, 15)

Table A.1: Parameters

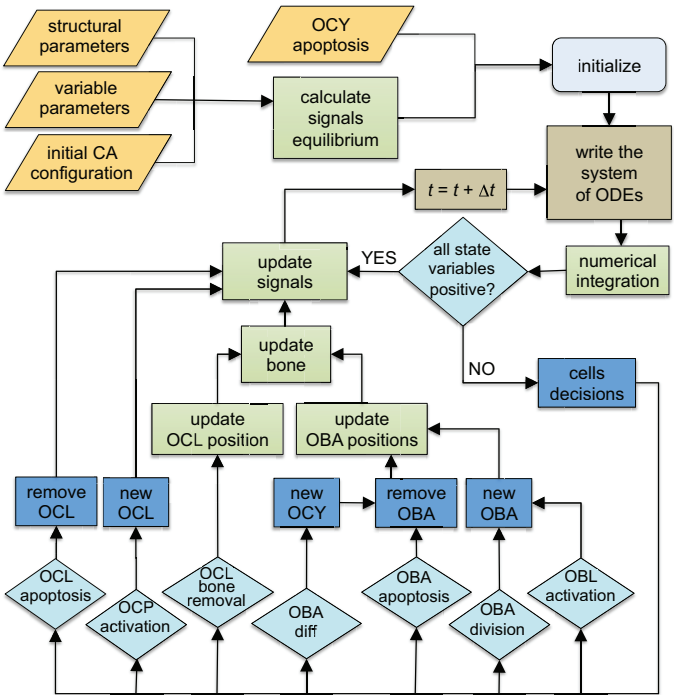


Figure A.3: Flowchart of the proposed model of BMU software as described in the Appendix.

Experimental procedure

Sixteen 10-week-old male Sprague-Dawley rats were obtained from the animal facility building of the University of Oviedo. Bone fractures with 2.5 mm average width were produced by the manual breakage using plate-bending devices, placed at the distal 3 third of the right tibia. The animal study protocol was approved by the local committee and conformed to Spanish animal protection laws. Rats were anesthetized and sacrificed by cervical dislocation 3, 6, 12 and 24 hours after fracture (n=5). Tibiae were isolated and cut through the sagittal plane of the metaphyseal fracture region into two equal sized parts and fixed by immersion in 4% paraformaldehyde at 4 C° for 12 h, rinsed in PBS, decalcified in 10% EDTA (pH 7.0) for 48 hours at 4 C°, dehydrated through a graded ethanol series, cleared in xylene and embedded in paraffin. Sections were serially cut at a thickness of 5 m, mounted on Superfrost Plus slides (Menzel-Glaser), stained with a trichromic method using Weigert's hematoxylin/alcian blue/picrofuchsin and viewed and photographed on a Nikon Eclipse E400 microscope.